Standardized Definition and Reporting of Vertical Resolution and Uncertainty in the NDACC Lidar Ozone and Temperature Algorithms.

Part 1: Vertical Resolution

T. Leblanc [1], R. Sica [2], A. van Gijsel [3], S. Godin-Beekmann [4], A. Haefele [5], T. Trickl [6], G. Payen[7], F. Gabarrot[7], and J. Bandoro[2]

[1] Jet Propulsion Laboratory, California Institute of Technology, Wrightwood, CA 92397, USA
[2] The University of Western Ontario, London, Canada
[3] Royal Netherlands Meteorological Institute (KNMI), Netherlands
[4] LATMOS-IPSL, CNRS-INSU, Paris, France
[5] Meteoswiss, Payerne, Switzerland
[6] Karlsruher Institut für Technologie, IMK-IFU, Garmisch-Partenkirchen, Germany
[7] Observatoire des Sciences de l'Univers de La Réunion, CNRS and Université de la Réunion (UMS3365), Saint Denis de la Réunion, France

Table of Contents

1 Introduction

The ISSI Team on NDACC Lidar Algorithms was formed to undertake the implementation of standardized definitions and approaches in several aspects of the retrieval of ozone (DIAL) and temperature (density integration technique) within NDACC. One of these aspects is vertical resolution. The purpose of providing vertical resolution in the data files together with a geophysical quantity is to provide information to the data user on the ability for the lidar instrument to detect geophysical features of specific vertical scale. Higher vertical resolution means that the instruments is able to detect features of small vertical extent, while lower vertical resolution implies a reduced ability to detect features of small vertical scale. Vertical resolution is provided in a unit of vertical length (e.g., meter), with the higher the vertical resolution, the smaller its numerical value.

The retrieval of temperature or atmospheric species from a lidar measurement starts with the lidar equation (e.g., Hinkley, 1976), which describes the emission of light by a laser source, its backscatter at altitude z, its extinction and scattering along its path up and back, and finally its collection on a detector. In **Part 2** of the present report, each term of this equation is described in details. Two important aspects of this equation are relevant to vertical resolution, first (to a first order approximation) the detected signal is proportional to the backscatter coefficient, which is proportional to the air number density, implying a large dynamic change in backscattered intensity between the lower and upper atmosphere (several orders of magnitude), and second, the signal is eventually limited by range and measurement sensitivity, causing detection noise to increase with altitude range.

In order to maximize the useful range of a noisy lidar-retrieved ozone or temperature profile, we can vertically filter the signal (or the species profile) to reduce the undesired noise. In the rest of this report, the word *filtering* is preferred to the word *smoothing* because it is more general and applies to both the smoothing and differentiation processes, the former process being relevant to both temperature and ozone retrievals, and the latter process being relevant to the ozone differential absorption technique. If the lidar signals or geophysical quantities derived from these measurements were not digitally filtered during the retrieval process, the vertical resolution would simply be equal to the instrument sampling resolution. However, most retrieved lidar parameters are digitally filtered at some point in the retrieval scheme. Over the years, NDACC lidar PIs have been providing temperature and ozone profiles using a wide range of vertical resolution schemes and definitions. The objective of the present work is not to recommend a specific vertical resolution scheme, but instead to make sure that the definition used by the data provider to describe his scheme is reported and interpreted consistently across the network. The approaches and recommendations in this report were designed so that they can be implemented consistently by all NDACC lidar investigators. We therefore recommend well-defined methods allowing a clear mapping of the amount of filtering applied to the lidar signal (or to the species profile) with the values of vertical resolution actually reported in the NDACC data files. Our report reviews a number of vertical resolution definitions used until now within the NDACC lidar community, and proposes to harmonize these definitions.

Section 2 summarizes the basics of digital signal filtering, and provides the main characteristics of commonly-used smoothing and derivative filters. **Section 3** presents examples of filters and vertical resolution definitions used by the NDACC ozone and temperature lidar community. The results from the first two sections are used in **section 4** to recommend two practical, well-known definitions of vertical resolution that can be easily linked to the underlying filtering processes.

One definition is based on the full-width at half-maximum of a finite impulse response, and the other definition is based on the cut-off frequency of digital filters. **Section 4** also describes numerical tools that were developed by the ISSI Team to facilitate the implementation of the proposed standardized definitions within the entire NDACC lidar community. The tools consist of subroutines written in three scientific languages (IDL, MATLAB and FORTRAN) which can be inserted in the NDACC investigators' data processing softwares in order to compute the proper, standardized numerical values of vertical resolution, based on the set of filter coefficients used.

The present recommendations for the standardization of the reporting of vertical resolution can be followed likewise for the retrieval of all species targeted by the NDACC lidars, i.e., ozone, temperature, water vapor, and aerosol backscatter ratio. One exception is when using an Optimal Estimation Method (OEM) for the retrieval of temperature as recently proposed by Sica and Haefele (2015), for which vertical resolution is determined from the Full-Width at Half-Maximum (FWHM) of the OEM's averaging kernels.

2 Brief review of signal filtering theory

Signal filtering for lidar data processing consists of either smoothing, differentiating or smoothing and differentiating at the same time. To describe the filtering process a signal S is defined in its general sense, i.e., it can be either a raw lidar signal from a single detection channel, or the ratio of the corrected signals from two detection channels, or an unsmoothed ozone profile, temperature profile, calibrated or uncalibrated water vapor profile, etc. The only common requirement is that the signal is formed of a finite number of equally-spaced samples in the vertical dimension $S(k)$ with $k=[1,nk]$. The constant interval between two samples, $\delta z = z(k+1)-z(k)$ for all k, is the *sampling width*, or *sampling resolution*, and corresponds to the smallest vertical interval that can be resolved by the lidar instrument.

In its most physical sense, the signal filtering process at an altitude $z(k)$ consists of convolving a set of $2N+1$ coefficients c_n with the signal S over the interval $\Delta z = 2N\delta z$ of boundaries $z(k-N)$ and $z(k+N)$:

$$S_f(k) = \sum_{n=-N}^{N} c_n S(k+n) \tag{2.1}$$

where S_f is the signal after filtering. The transformation associated with this process is known as a non-recursive digital filter the simplest kind of digital filters, with the coefficients c_n being the coefficients of the filter. A simple example is the arithmetic running average, for which all coefficients take the same value $c_n = 1/(2N+1)$. Several other names exist for this linear combination, for example boxcar smoothing filter, boxcar function and smoothing by [2N+1]s. The number of filter coefficients and the values of these coefficients determine the actual effect of the filter on the signal. Three critical aspects of the effect of the filter on the signal are 1) the amount of noise reduction due to filtering, 2) the nature and degree of symmetry/asymmetry of the coefficients around the central value which determines whether the filter's function is to smooth, sum, differentiate, or interpolate, and 3) whether the magnitude of specific noise frequencies are being amplified or reduced after filtering.

In the particular case of an unfiltered signal comprised of independent samples and assuming that the variance of the noise for the unfiltered signal is constant through the filtering interval considered ($\sigma_S^2(k') = \sigma^2$ for all k' in the interval $[k-N,k+N]$), we obtain a simple relation that estimates the variance of the output signal:

$$\sigma_{Sf}^2(k) = \sigma_S^2 \sum_{n=-N}^{N} c_n^2 \tag{2.2}$$

This relation reveals the importance of the sum of the squared-coefficients to determine the amount of noise reduction. However, it does not provide any information on the ability of the filter to distinguish what is noise and what is actual signal. To illustrate this problem, **Figure 2.1** shows an example of a noisy signal before and after filtering, considering two different filters. We start from a modeled signal represented by the green dash-dot curve. To this ideal signal, we add random noise which amplitude is distributed following the Poisson statistics (signal detection noise). The noisy "unfiltered" signal is represented in this figure by a dark-grey dotted curve. The signal is then filtered using two different filters, i.e., two different sets of coefficients. The blue curve shows the filtered signal using least squares linear fitting (identical to boxcar average, labeled LS-1), while the red curve shows the filtered signal this time using least squares fitting with a polynomial of degree 2 (LS-2). The number of terms used by both filters is the same ($2N+1=11$). The values of the coefficients, and not the number of coefficients, are responsible for the observed difference.

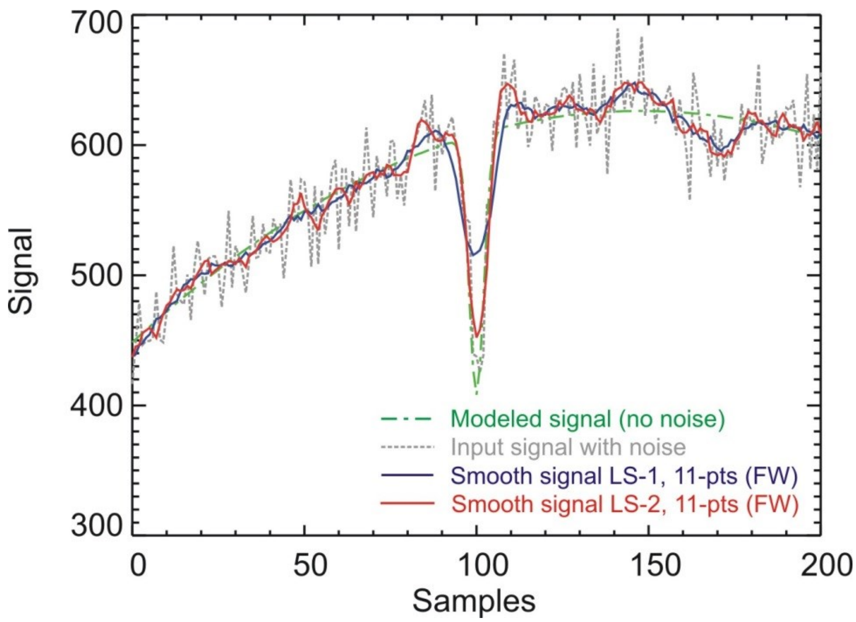

Figure 2.1 Example of the differing impact of two smoothing filters of identical number of terms ($2N+1=11$). The green dot-dash curve is the modeled signal (with no noise), the grey dotted curve is the modeled input signal containing Poisson noise, the blue and red curves are the smoothed signal using a 11-pts boxcar average (LS-1) and the Least –squares fitting method with a polynomial of degree 2 (LS-2) respectively

In the real world, we typically do not know the exact nature or behavior of the measured signal. Consider the example in **Figure 2.1**, if the definition used to report vertical resolution in the NDACC data files was based on the number of points used by the filter, we would not be able to attribute the differences observed between the blue and red curves to a difference in the filtering procedure. We therefore need to find some analytical way to characterize a specific filter if we want to understand its exact effect on the signal, and properly interpret features observed on the smoothed signal. We will see thereafter that it is indeed possible to determine the resolution of the filter by either quantifying the response of a controlled impulse in the physical domain, or by using a frequency approach and studying the frequency-response of the filter.

2.1 Classical approach: Unit impulse response and unit step response

The impact of a specific filter on the signal can be characterized by computing the unit impulse response in the physical domain (usually called the time domain in time series analysis). This can be done by using a well-known, controlled input signal, e.g., an impulse, and by studying its response after being convolved by the filter coefficients. Considering a finite impulse response is equivalent to considering the output signal I_{OUT} formed by the convolution of an impulse I_{INP} with a finite number of coefficients c_n:

$$I_{OUT}(k) = \sum_{n=-N}^{N} c_n I_{INP}(k+n) \tag{2.3}$$

For smoothing, non-derivative filters, this impulse is the discrete Kronecker delta function δ_{k0} (also called unit impulse function), which takes a value of 1 at coordinate $k=k_0$ and 0 elsewhere:

$$\delta_{k0}(k) = 1 \qquad \text{for } k = k_0$$

$$\delta_{k0}(k) = 0 \qquad \text{for all } k \neq k_0 \tag{2.4}$$

Using our smoothing interval of $2N+1$ points centered at altitude $z(k)$, the input impulse for which the response is needed will have a value of 1 at the central point, and 0 at all other points:

$$I_{INP}(k+n) = 1 \qquad \text{for } n = 0$$

$$I_{INP}(k+n) = 0 \qquad \text{for } 0 < |n| \leq N \tag{2.5}$$

For derivative filters, we are interested in the response of a discrete Heaviside step function H_S (also called unit step function), which takes a value of 0 for all strictly negative values of k, and a value of 1 elsewhere:

$$H_S(k) = 0 \qquad k < 0$$

$$H_S(k) = 1 \qquad k \geq 0 \tag{2.6}$$

Again using an interval of $2N+1$ points centered at $z(k)$, the input step for which the response is needed will have a value of 0 for all samples below the central point $z(k)$, and a value of 1 for the central point and all samples above it:

$$I_{INP}(k+n) = 0 \qquad -N \leq n < 0$$

$$I_{INP}(k+n) = 1 \qquad 0 \leq n \leq N \tag{2.7}$$

Though we considered an impulse (delta function) for smoothing filters and a step function (Heaviside step) for the derivative filters, for brevity we will call both types of response an "*impulse response*" in the rest of this report. For each altitude location considered, the impulse response consists of a vector which length is at least as large as twice the number of filter coefficients used to smooth the signal at this location. The magnitude of the impulse response typically maximizes at the central point $z(k)$ of the filtering interval, and then decreases apart from this central value to a value of 0 for points outside the smoothing interval. Unlike the number of coefficients used by the filter, the width of the response (measured in number of bins) provides a quantitative measure of the actual smoothing impact of the filter on the signal at this location. Several examples of impulse response are discussed in **sections 2.3 and 2.4**.

2.2 The frequency approach: Transfer function and gain

As in many signal processing applications, the frequency approach applied to lidar signal filtering or lidar-retrieved profile filtering is a very convenient mathematical framework. It is a more abstract, but very powerful tool allowing to understand many hidden features of the smoothing and differentiation processes. A succinct, yet clear discussion of the required mathematical background is provided by Hamming (1989). Here, we will provide a brief review of this background relevant to our applications.

1) *Aliasing*: Any signal consisting of a finite number of equally-spaced samples in the physical domain is an aliased representation of a sine and cosine function of frequency ω. Using the usual trigonometry formulae and the Euler identity, we can therefore express the signal in complex form:

$$S(k) = e^{i\omega k} \tag{2.8}$$

In the case of lidar, the signal (or the ozone or temperature profile) is a function of altitude range. The discretized independent variable is the vertical sampling bin k. The angular frequency ω (unit: radian.bin^{-1}) is then connected to the frequency f (unit: bin^{-1}) and vertical wavelength L (unit: bin) by the relations:

$$\omega = 2\pi f = \frac{2\pi}{L} \tag{2.9}$$

2) *Eigen-functions and eigenvalues of a linear system*: Any vector **x** of length M can be formed by linear combination of M linearly independent (orthogonal) eigenvectors $\boldsymbol{x}_i$:

$$\mathbf{x} = \sum_{i=1}^{M} a_i \mathbf{x}_i \tag{2.10}$$

Furthermore, any non-zero and non-unity matrix **A** of dimension M by M multiplied by this vector can be expressed as the sum of the products of its elements by the corresponding eigenvalues λ_i:

$$\mathbf{Ax} = \sum_{i=1}^{M} a_i \mathbf{Ax}_i = \sum_{i=1}^{M} a_i \lambda_i \mathbf{x}_i \tag{2.11}$$

3) *Invariance under translation*: The property of invariance under translation for the sine and cosine functions implies a direct relation between the signal expressed in its complex form and the eigenvalue $\lambda(\omega)$ for a given translation:

$$S(k+n) = e^{i\omega(k+n)} = e^{i\omega n} e^{i\omega k} = \lambda(\omega) S(k) \tag{2.12}$$

Using the above mathematical background, the filtered signal S_f presented in its classical form as a linear combination of the input signal S (**Eq. (2.1)**) can be re-written in its frequency-approach form:

$$S_f(k) = e^{i\omega k} \sum_{n=-N}^{N} c_n e^{i\omega n} = \lambda(\omega) e^{i\omega k} = \lambda(\omega) S(k)$$

(2.13)

The eigenvalue $\lambda(\omega)$ is independent of *k*, and is called the *transfer function*, which can be computed in the frequency domain over a full cycle [-π,π], or over half a cycle [0,π] without losing information (symmetry of translation):

$$\lambda(\omega) = \sum_{n=-N}^{N} c_n e^{i\omega n} \qquad 0 \le \omega \le \pi \ \text{ radian.bin}^{-1}$$

(2.14)

We can express the transfer function more conveniently as a function of the frequency *f*:

$$H(f) = \sum_{n=-N}^{N} c_n e^{2i\pi fn} \qquad 0 \le f \le 0.5 \ \text{bin}^{-1}$$

(2.15)

The maximum value $f = 0.5$ bin^{-1} is the Nyquist frequency, which corresponds to L=2 bins, and which expresses the fact that the lidar instrument is unable to fully resolve any feature of vertical wavelength smaller than twice the sampling resolution ($2\delta z$). The transformation described in **Eq.(2.15)** can easily be recognized as a well-known discrete Laplace Transform, applied to the filter coefficients.

For a typical smoothing filter, the coefficients have even symmetry, i.e., $c_n = c_{-n}$ for all values of *n*. The complex transfer function can then be reduced to its real part. The gain of the filter *G*, which is the ratio of the actual transfer function $H(f)$ to the ideal transfer function $I(f)$ can then be written:

$$G(f) = \frac{H(f)}{I(f)} = \frac{H(f)}{1} = c_0 + 2\sum_{n=1}^{N} c_n \cos(2\pi nf) \qquad 0 \le f \le 0.5 \ \text{bin}^{-1}$$

(2.16)

For a derivative filter, the $2N$+1 coefficients have odd symmetry, i.e., $c_n = -c_{-n}$ for all values of *n* and $c_0 = 0$. The complex transfer function is then reduced to its imaginary component:

$$H(f) = 2i\sum_{n=1}^{N} c_n \sin(2\pi nf)$$

With the complex notation of **Eq. (2.8)**, the ideal vertical derivative of the signal can be written:

$$S_f(k) = i\omega e^{i\omega k} = 2i\pi f e^{i\omega k}$$

(2.17)

The gain of the filter, i.e., the ratio of the actual transfer function to the ideal transfer function, then takes the form:

$$G(f) = \frac{H(f)}{2i\pi f} = \frac{1}{\pi f}\sum_{n=1}^{N} c_n \sin(2\pi nf) \qquad 0 \le f \le 0.5 \ \text{bin}^{-1}$$

(2.18)

2.3 Impulse response and gain of commonly-used smoothing filters

Here we briefly review, only for reference, a few commonly-used smoothing filters. Providing recommendations for the use of specific filters is beyond the scope of the ISSI-Team work. However, inspection of the many transfer functions shown in this section can help the reader in the design of a filter optimized for his application.

2.3.1 Least squares fitting, boxcar average, and smoothing by *n*s

Least-squares fitting is a well-established numerical technique used for many applications such as signal smoothing, differentiation, interpolation, etc.. The relation between the number and values of the filter coefficients and the type of polynomial used to fit the signal can be found in many text books and publications (e.g., Birge et al., 1947; Savitsky and Golay, 1964; Steinier et al., 1972). In this paragraph we show that *least-squares fitting* with a straight line, *boxcar averaging* and *smoothing by ns*, are all the same filter. We start with the simple case of fitting five points with a straight line. We therefore look for the minimization of the following function:

$$F(a_0, a_1) = \sum_{n=-2}^{2} \left[S(k+n) - (a_0 + a_1 n) \right]^2 \tag{2.19}$$

This minimization is done by differentiating F with respect to each coefficient a_0 and a_1 and finding the root of each corresponding equation:

$$\begin{cases} 5a_0 + 0a_1 = \sum_{n=-2}^{2} S(k+n) \\ 0a_0 + 10a_1 = \sum_{n=-2}^{2} nS(k+n) \end{cases} \tag{2.20}$$

The value of the signal after filtering S_f is the mid-point value of the fitting function a_0+a_1n which corresponds to the value of a_0 (n=0):

$$S_f(k) = a_0 = \frac{1}{5} \sum_{n=-2}^{2} S(k+n) \tag{2.21}$$

Identifying this equation to the generic **Eq. (2.1)**, we deduce the five coefficients of the filter:

$$c_n = \frac{1}{5} \qquad -2 \le n \le 2$$

We recognize the smoothing-by-5s filter or 5-point boxcar average, or 5-pts running average. The impulse response of this filter takes a value of 1 for all $|n|$ comprised between 0 and N, and a value of 0 elsewhere (see **Figure 2.2**, left plot). Not surprisingly, all impulse response curves maximize at the central point (n=0), and their full-width at half-maximum (FWHM) increases with the number of filter coefficients used.

Now switching to the frequency domain and using **Eq. (2.14)**, the transfer function $\lambda(\omega)$ can be written in complex form:

$$\lambda(\omega) = \frac{1}{5}\left[e^{-2i\omega} + e^{-i\omega} + 1 + e^{i\omega} + e^{2i\omega}\right]$$

(2.22)

The gain of the filter can be expressed as a function of frequency f:

$$G(f) = H(f) = \frac{1}{5} + 2\sum_{n=1}^{2}\frac{1}{5}\cos(2\pi nf)$$

which simplifies to:

$$G(f) = H(f) = \frac{1}{5}\left[\frac{\sin(5\pi f)}{\sin(\pi f)}\right]$$

(2.23)

We can generalize the above equation by fitting $2N$+1 points with a straight line, and we find:

$$c_n = \frac{1}{2N+1} \qquad -N \le n \le N$$

$$\lambda(\omega) = \frac{1}{2N+1}\left[e^{-Ni\omega} + e^{-(N-1)i\omega} + \ldots + e^{-i\omega} + 1 + e^{i\omega} + \ldots + e^{(N-1)i\omega} + e^{Ni\omega}\right]$$

(2.24)

Or in function of frequency:

$$G(f) = H(f) = \frac{1}{2N+1} + 2\sum_{n=1}^{N}\frac{\cos(2\pi nf)}{2N+1}$$

which simplifies to

$$G(f) = H(f) = \frac{1}{2N+1}\left[\frac{\sin\left((2N+1)\pi f\right)}{\sin(\pi f)}\right]$$

(2.25)

The gains for smoothing by 3s through 25s filters are plotted on the right-hand side of **Figure 2.2**. The gain provides a more complete description of the smoothing ability of the filters because it provides a measure of noise attenuation as a function of frequency. All curves show a gain close to 1 for frequency values near 0 (low-pass filters), but they also show large wiggles at larger frequencies when we approach the Nyquist frequency. The frequency f_0 of the first zero-crossing (zero-gain) is determined by the number of points used:

$$f_0 = \frac{1}{2N+1}$$

(2.26)

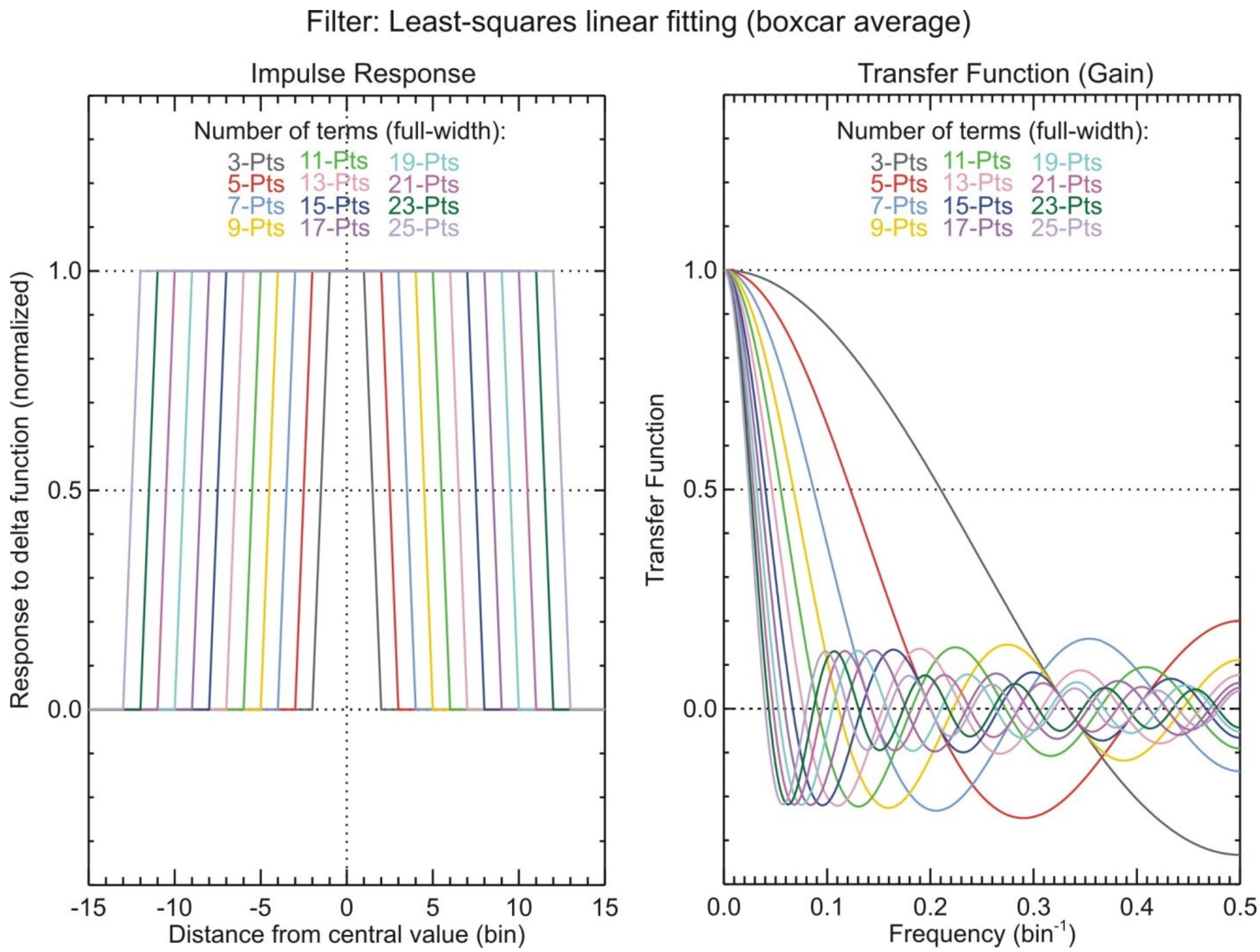

Figure 2.2 Impulse response (left) and gain (right) for a digital filter equivalent to fitting an unsmoothed signal with a polynomial of degree 1 or 2 using the least-squares method over an interval comprising 2*N*+1 points (full width). Full widths represented in this figure range from 3 to 25 points. This least-squares filtering procedure is equivalent to a running average over 2*N*+1 points (full width) as well as smoothing by (2*N*+1)s

The wiggles observed on the right-hand side plot of **Figure 2.2** (the Gibbs phenomenon) are undesirable if the filter's objective is to remove the highest frequencies from the signal, which is the case for the lidar signal impacted by detection noise. The Gibbs ripples are predicted by the Fourier theory because these digital filters have a finite number of coefficients, the equivalent in the physical domain of truncated Fourier series in the frequency domain. The strength of the frequency approach is to use the Fourier theory, and in particular the concept of windowing, to minimize the Gibbs ripples. Detailing the underlying theory behind this behavior is beyond the scope of the present report. Instead, we will simply provide here the most common examples of modifications made to the filter coefficients allowing an optimized design of a noise-reduction filter. More details on filters windows can be found for example in Rabiner and Gold (1979).

2.3.2 Modified least squares

In this first example we modify the shape of the transfer function by changing the two terms at the end of the summation, more specifically, taking half of the value of the end coefficients instead of their full value. We also need to re-normalize the sum of the coefficients to $2N$ instead of $2N+1$, and we obtain the transfer function for the so-called *modified least-squares*:

$$\lambda(\omega)=\frac{1}{2N}\left[\frac{1}{2}e^{-Ni\omega}+e^{-(N-1)i\omega}+\ldots+e^{-i\omega}+1+e^{i\omega}+\ldots+e^{(N-1)i\omega}+\frac{1}{2}e^{Ni\omega}\right] \tag{2.27}$$

Leading to:

$$G(f)=H(f)=\frac{1}{2N}\left[\frac{\sin\left((2N+1)\pi f\right)}{\sin(\pi f)}-\cos(2\pi Nf)\right]=\frac{1}{2N}\left[\frac{\sin(2\pi Nf)\cos(\pi f)}{\sin(\pi f)}\right] \tag{2.28}$$

With the presently modified coefficients, the frequency f_0 of the position of the first zero-gain node is now:

$$f_0=\frac{1}{2N}$$

Figure 2.3 shows the impulse response (left) and the gain (right) for the modified least-squares filters with a full-width comprised between 3 and 25 points. As can be seen on the right-hand side plot, changing the two end coefficients has the effect of producing a slightly less efficient low-pass filter (f_0 is increased) but a more efficient high-stop filter (i.e., smaller amplitude of the Gibbs ripples).

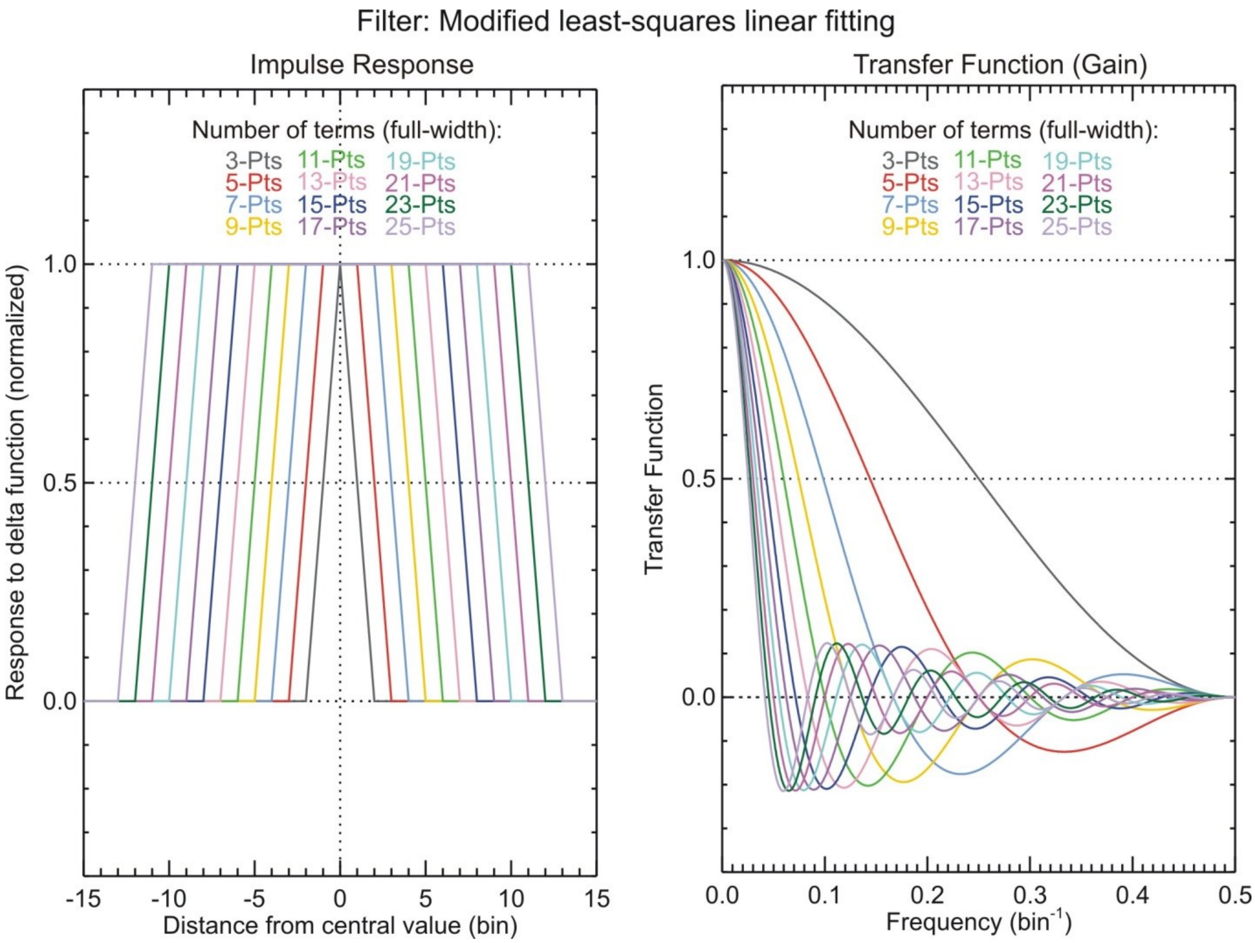

Figure 2.3 Same as Figure 2.2, but after halving the values of the two end coefficients (modified least-squares, see text for details)

2.3.3 Low-pass filter and cut-off frequency

If we were to consider an ideal low-pass filter with an infinite number of terms, the theoretical transfer function would have values strictly comprised between 0 and 1 representing the perfect gain of the filter (no ripples). The so-called *transition region* corresponds to the region where we want the transfer function to drop from a value of 1 at lower frequencies to a value of 0 at higher frequencies. The width of the transition region is the *bandwidth*. We can define the *cut-off frequency* of a low-pass filter as the frequency at which the transfer function equals 0.5. For most low-pass filters this is at the center of the bandwidth. To design a low-pass filter with the desired cut-off frequency f_C, we start with the initial conditions defining an ideal low-pass filter:

$$G(f) = 1 \qquad \text{for } 0 < |f| < f_C$$

$$G(f) = 0 \qquad \text{for } f_C < |f| < 0.5$$

$$G(f) = G(-f) \tag{2.29}$$

Without getting into mathematical details, we find that these conditions are always true for a family of un-truncated Fourier series with the following transfer function:

$$H(f) = 2f_C + 2\sum_{n=1}^{\infty} \frac{\sin(2\pi n f_C)}{\pi n} \cos(2\pi n f) \tag{2.30}$$

Since we have to work with a finite number of samples, we truncate the series to a finite number of terms at the expense of producing Gibbs ripples. The real-world low-pass filter thus created has the following $2N$+1 coefficients and transfer function:

$$c_n = 2f_C \frac{\sin(2\pi n f_C)}{2\pi n f_C} \qquad -N \le n \le N \tag{2.31}$$

$$G(f) = H(f) = 2f_C + 2\sum_{n=1}^{N} \frac{\sin(2\pi n f_C)}{\pi n} \cos(2\pi n f) \tag{2.32}$$

An example, for f_c=0.15, is provided for reference in **Figure 2.4**. The impulse response (left) and gain (right) are shown for a filter full-width comprised between 3 and 25 points. The first few Gibbs ripples always have the largest amplitude. Using a higher number of terms causes the ripples to be more concentrated near the transition region, and causes higher orders' ripples with a smaller amplitude to occur near the Nyquist frequency

The gain curves show that the transition region is narrower than that observed for the *smoothing by ns* filters, but the Gibbs ripples appear on both sides of the transition region. Just like for the modified least squares fitting, we can reduce the magnitude of the Gibbs ripples by modifying the filter coefficients, specifically by applying additional weights to the filter coefficients, a process called *windowing*.

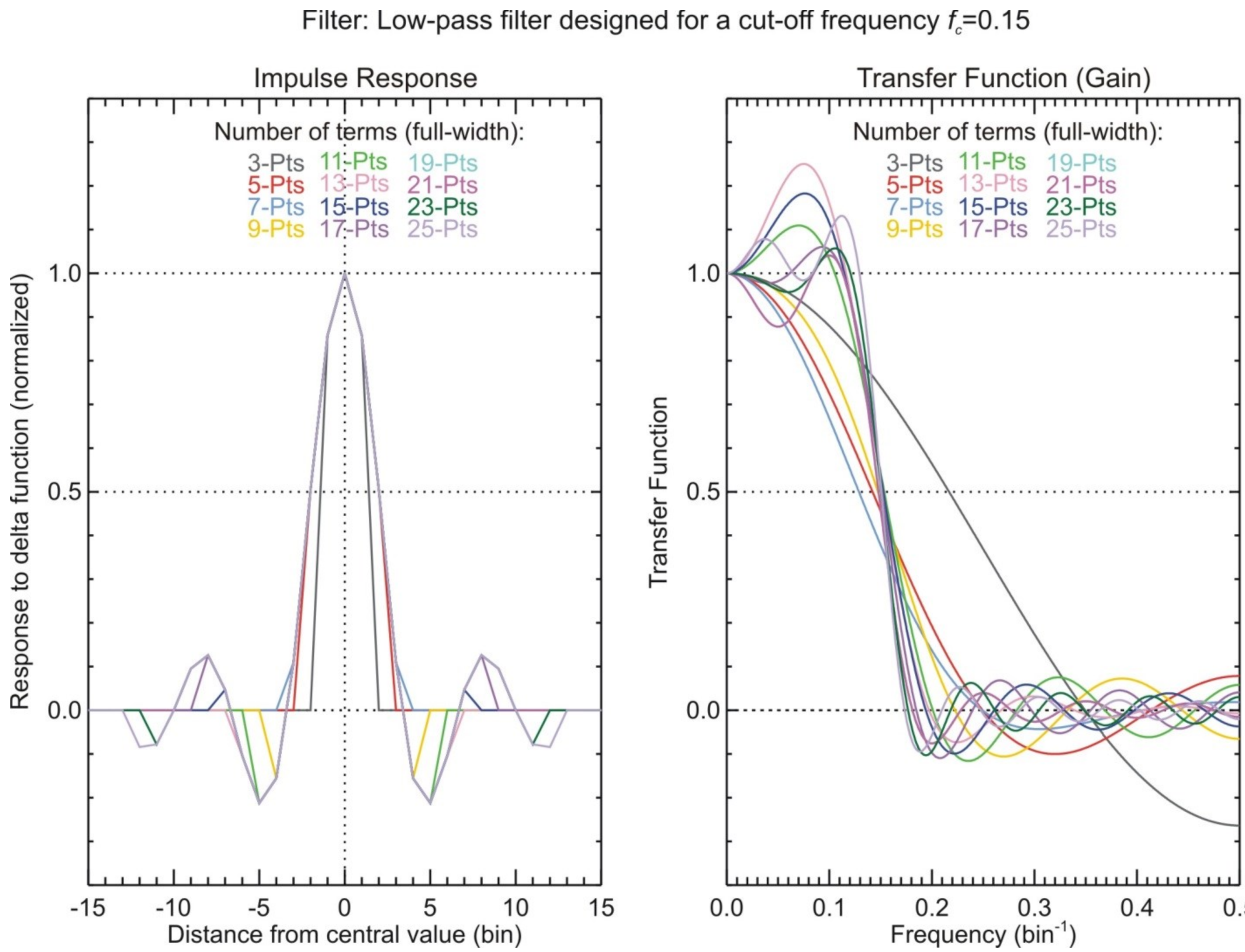

Figure 2.4 Impulse response and gain of low-pass filters using 2*N*+1 coefficients (full width), and designed to have a cut-off frequency f_c=0.15. Full widths range from 3 to 25 points

2.3.4 Lanczos window

The windowing procedure consists of applying well-chosen additional weights to the original filter coefficients in order to change the shape of the transfer function (in our case, to reduce the amplitude of the Gibbs ripples). For example it can be shown (Hamming, 1989) that a discrete Fourier series truncated at its M^{th} term could be efficiently smoothed (and therefore Gibbs ripples attenuated) if its coefficients were multiplied by the so-called *sigma factors*. For a smoothing filter with even symmetry, an unsmoothed, *M*-terms truncated discrete Fourier series can be written:

$$F(f) = c_0 + 2\sum_{n=1}^{M} c_n \cos(2\pi nf) \qquad \textbf{(2.33)}$$

The sigma factors can be written:

$$\sigma(M,n) = \frac{\sin(\pi n / M)}{(\pi n / M)} \qquad 1 \le n \le M$$

(2.34)

The smoothed Fourier series can then be written:

$$F_S(f) = c_0 + 2\sum_{n=1}^{M} \sigma(M,n) c_n \cos(2\pi nf) \tag{2.35}$$

Considering the low-pass filter case with $2N$+1 coefficients (full width), the sigma factors are then:

$$w_n = \frac{\sin(\pi n / N)}{(\pi n / N)} \qquad -N \le n \le N \tag{2.36}$$

Note that the sigma factor at the central location (n=0) is $\sigma(N,0)=1$. The new filter coefficients and transfer function can now be written:

$$c_n = 2f_C \frac{\sin(2\pi nf_C)}{2\pi nf_C} w_n = 2f_C \frac{\sin(2\pi nf_C)}{2\pi nf_C} \frac{\sin(\pi n / N)}{\pi n / N} \qquad -N \le n \le N \tag{2.37}$$

$$G(f) = H(f) = 2f_C + 2\sum_{n=1}^{N} \frac{\sin(2\pi nf_C)}{\pi n} \frac{\sin(\pi n / N)}{(\pi n / N)} \cos(2\pi nf) \tag{2.38}$$

Figure 2.5 shows the impulse response (left) and gain (right) of the low-pass filter introduced in the previous paragraph, this time with its coefficients weighted by the Lanczos window (full-width comprised between 3 and 25 points). The convolution of the low-pass filter coefficients by the Lanczos window reduces greatly the Gibbs ripples. Note that the 3-point Lanczos window consists of two null coefficients and one unity coefficient, which is equivalent to no filtering and results into a gain equal to 1 at all frequencies. We kept it on the figure only for the sake of completeness.

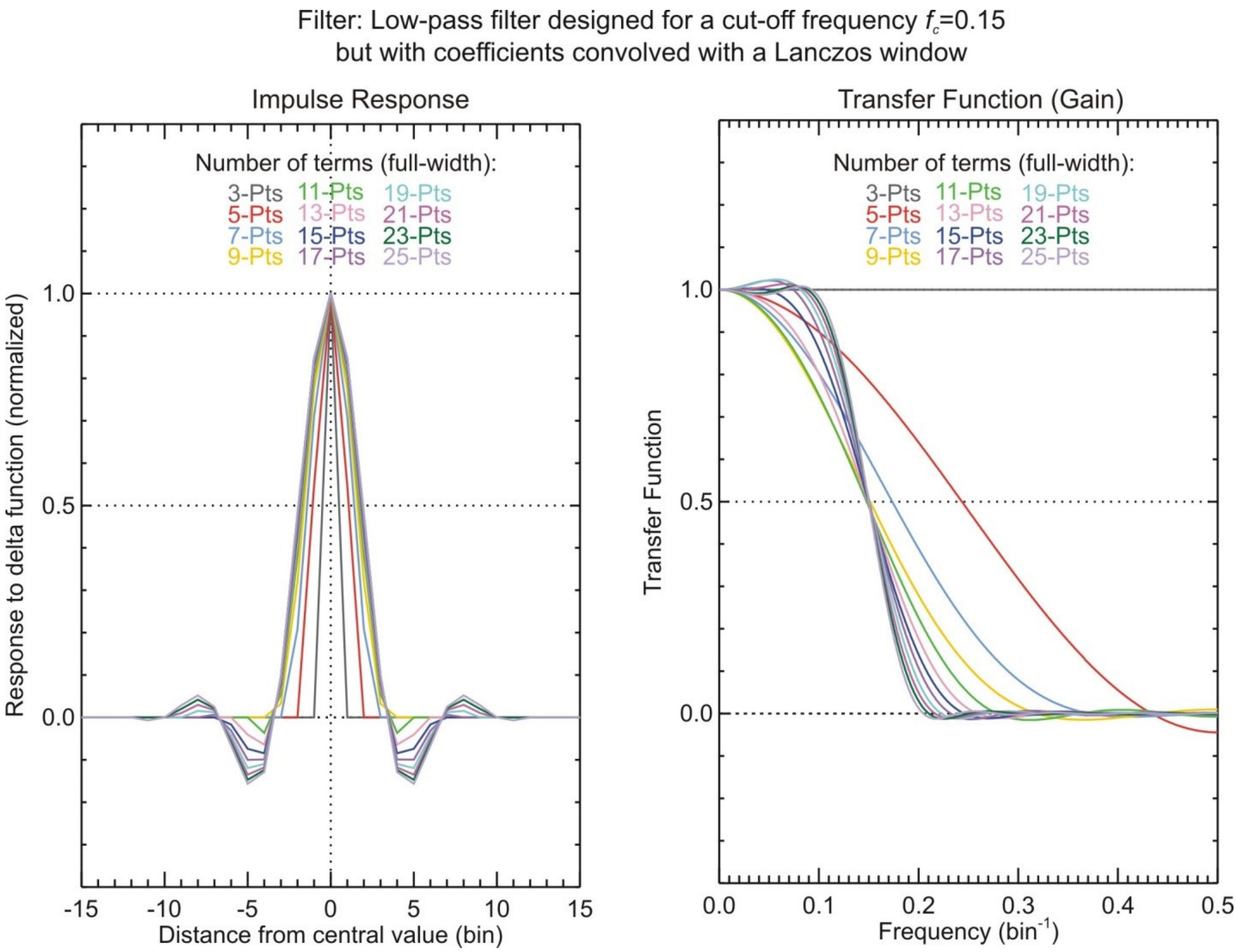

Figure 2.5 Same as Figure 2.4, this time after the low-pass filter coefficients were convolved with a Lanczos window

2.3.5 Von Hann window (or Hanning, or raised cosine window)

Another window commonly used is the von Hann window (also called Hanning window or the raised cosine window). For a window of $2N$+1 terms, the window weights in this case are defined by:

$$w_n = \frac{1 + \cos(\pi n / N)}{2} \qquad -N \le n \le N \tag{2.39}$$

Figure 2.6 shows the impulse response (left) and gain (right) of the box car average filter after it is convoluted by the von Hann window.

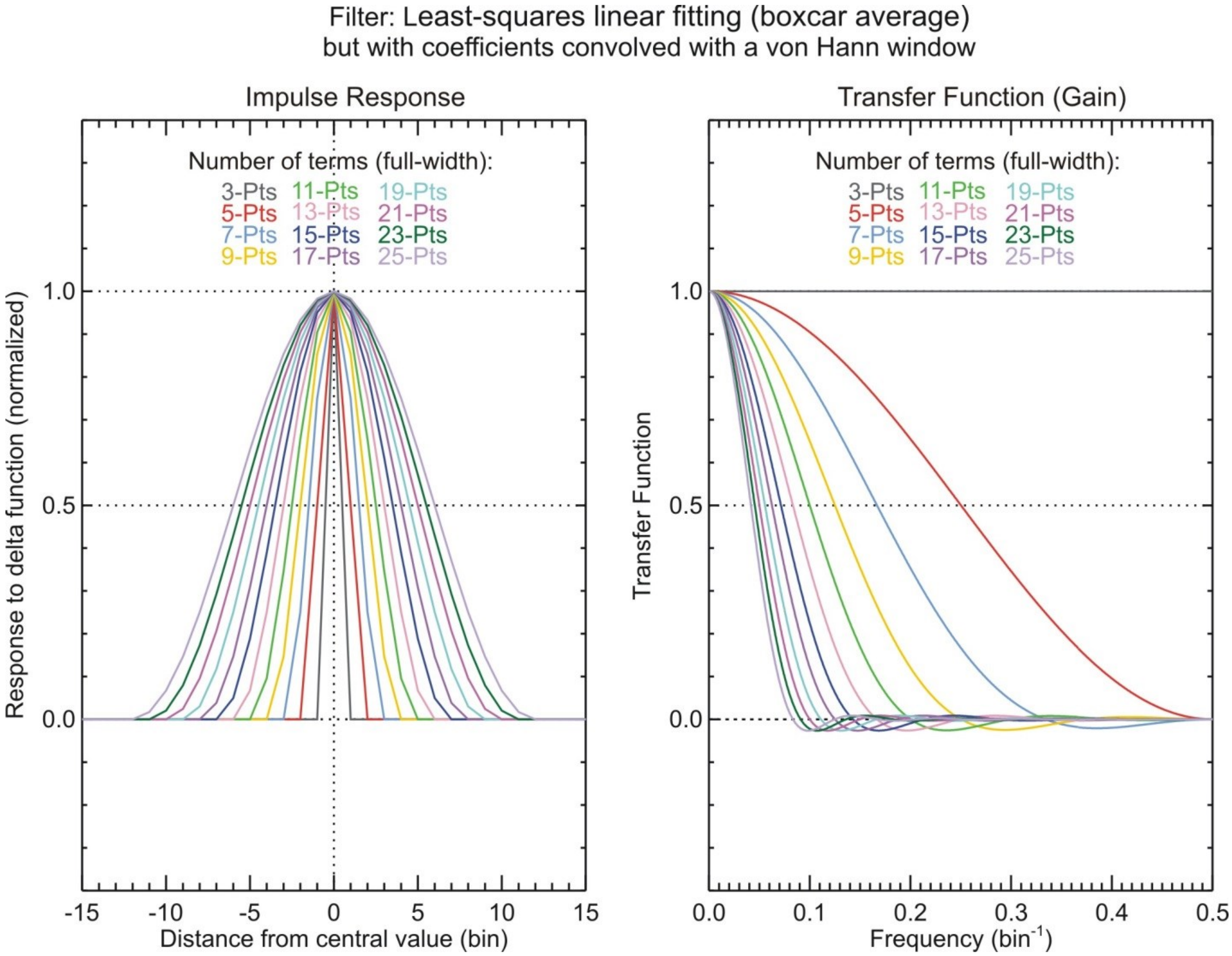

Figure 2.6 Same as Figure 2.2, but this time after the boxcar filter coefficients were convolved with a von Hann window

Using this window causes the transition region to be much wider, but the Gibbs ripples to have a much smaller amplitude. The frequency f_0 of the first node (zero-gain) is now:

$$f_0 = \frac{1}{N} \tag{2.40}$$

2.3.6 Hamming window

The sign of the lobes of the Von Hann window transfer function is opposite to those of the least-square transfer function (not shown). The Hamming window consists of finding the optimized linear combination of these two transfer functions that will minimize the magnitude of those lobes. The result is a slightly modified version of the von Hann window:

$$w_n = \alpha + \beta \cos(\pi n / N) \qquad \text{with } \alpha + 2\beta = 1 \qquad -N \le n \le N \tag{2.41}$$

Contrary to common belief, α and β are not constants. They represent only approximations of the best solution for the minimization of the lobes amplitude, and their value depends on N. For large values of N, we find $\alpha = 0.54$ and $\beta = 0.23$, but for small values ($N < 6$) we find $\alpha > 0.55$ and $\beta < 0.225$ (Hamming, 1989).

2.3.7 Blackman window

We can continue to follow the same approach to minimize further the amplitude of the Gibbs ripples by taking optimized linear combinations of the rectangular and cosine window functions, this time using higher harmonics. One common window obtained this way is the Blackman window, defined by its weights:

$$w_n = \alpha + \beta \cos(\pi n / N) + \chi \cos(2\pi n / N) \qquad -N \le n \le N \tag{2.42}$$

This time, we have α=0.42, β=0.42, and χ=0.08.

2.3.8 Kaiser window and NER filter

An alternate set of window weights was suggested by Kaiser and Reed (1977). These weights have the main function of spreading the large amplitude of the first Gibbs ripples (those near the transition region) into all the ripples between the transition region and the two ends of the frequency range (f=0 and f=0.5). The weights are based on the Bessel function I_0, and can be written:

$$w_n = \frac{I_0\left(\alpha\sqrt{1-(n/N)^2}\right)}{I_0(\alpha)} \qquad -N \le n \le N \tag{2.43}$$

with the Bessel function:

$$I_0(\alpha) = 1 + \sum_{m=1}^{\infty}\left(\frac{(\alpha/2)^m}{m!}\right)^2 \tag{2.44}$$

The convolution of the Kaiser window weights with the boxcar filter coefficients results in the so-called Near-Equal-Ripple (NER) filter:

$$c_n = 2f_C \frac{\sin(2\pi n f_C)}{2\pi n f_C} w_n = 2f_C \frac{\sin(2\pi n f_C)}{2\pi n f_C} \frac{I_0\left(\alpha\sqrt{1-(n/N)^2}\right)}{I_0(\alpha)} \tag{2.45}$$

The advantage of this filter is the ability to fine-tune the cut-off frequency, the bandwidth and the amplitude of the Gibbs ripples, all at the same time. Obviously the method does not produce a "perfect" filter, but it allows the optimization of at least two filter parameters at the expense of the third one. For example, we can prescribe the bandwidth of the transition region Δf_C (full-width) with $\Delta f_C < 2f_C$ and $\Delta f_C < 1\text{-}2f_C$, and the amplitude of the Gibbs ripples δ (half-width), and deduce the number of filter coefficients needed. Following the formulation of Kaiser and Reed (1977), the amplitude of the Gibbs ripples can be expressed in terms of attenuation A (in decibel):

$$A = -20\log_{10}(\delta) \tag{2.46}$$

After we fix the attenuation A and bandwidth Δf_C, an optimal Kaiser filter will be designed by calculating the required number of points N (half-width) using:

$$N = \text{int}\left(\frac{0.13927(A-7.95)}{4\Delta f_C} + 0.75\right) \quad \text{for } A > 21$$

$$N = \text{int}\left(\frac{1.8445}{4\Delta f_C} + 0.75\right) \quad \text{for } A < 21 \tag{2.47}$$

The α parameter used in argument of the Bessel function is then computed using:

$$\alpha = 0.1102(A-8.7) \quad \text{for } A > 21$$

$$\alpha = 0.5842(A-21)^{0.4} + 0.07886(A-21) \quad \text{for } 21 < A < 50$$

$$\alpha = 0 \quad \text{for } A < 21 \tag{2.48}$$

An example of optimized low-pass filter using a Kaiser window with 50-dB attenuation is provided in **Figure 2.7**. Once again the impulse response is on the left, and the gain is on the right. The right-hand plot shows that the total number of coefficients $2N+1$ must be 7 or larger to produce an optimized filter for this particular value of attenuation.

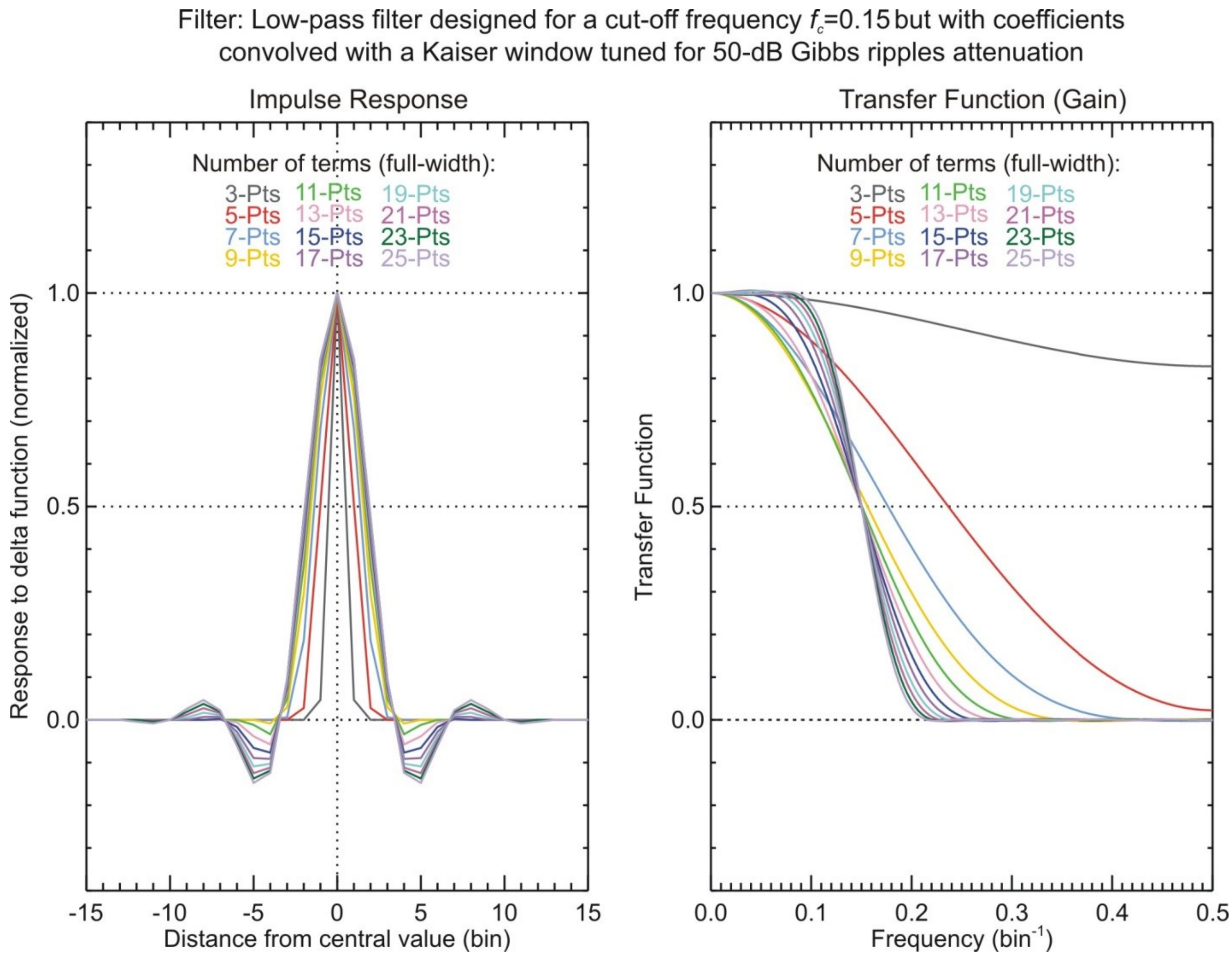

Figure 2.7 Same as Figure 2.5, this time after the low-pass filter coefficients were convolved with a 50-dB attenuation Kaiser window

2.3.9 Noise reduction and number of filter coefficients

Figure 2.8 shows, for four of the filters introduced in this section, the amount of noise reduction as a function of the number of filter coefficients used. The noise reduction values are computed using **Eq. (2.2)**. The black dotted curve on each plot shows the noise reduction expected from an arithmetic average of multiple samples containing Poisson-distributed noise (i.e., square root of the number of samples used for the average). Not surprisingly, it is identical to the red symbols on the top-left figures (boxcar average). The bottom-left and top-right plots show that higher orders polynomials, or filters convolved with windows, yield a noisier signal (less noise reduction) than in the case of the simple boxcar average. The bottom-right plot shows that noise reduction for low-pass filters designed with a prescribed cut-off frequency does not increase with the number of coefficients used.

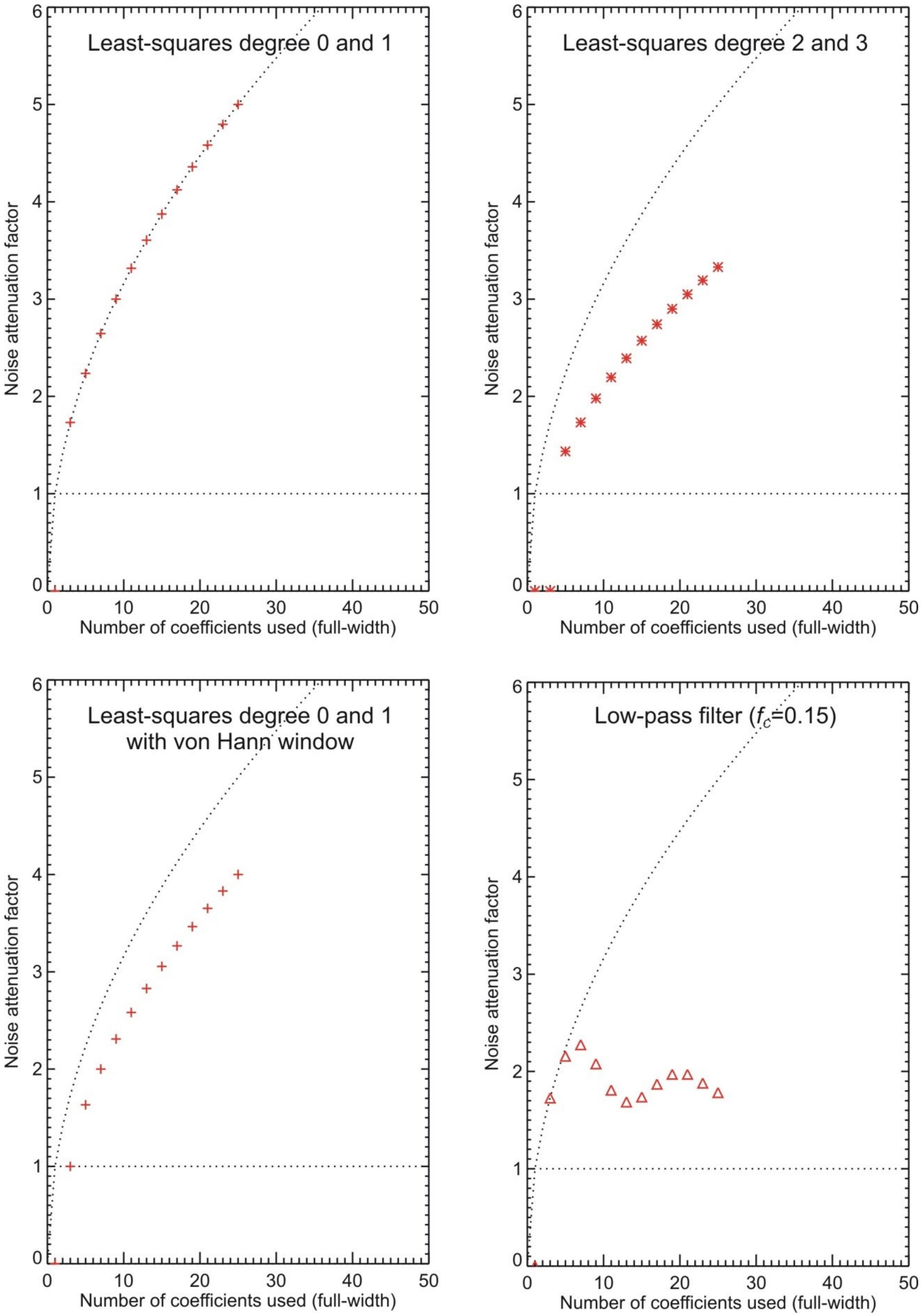

Figure 2.8 Noise reduction factor as a function of the number of coefficients, for a selected number of filters introduced in the previous section (see text for details)

Table 2.1 Noise reduction factor (normalized to sqrt(2N+1)) for the least-squares fitting smoothing filters and windows introduced in this section

Noise reduction/sqrt(2*N*+1)	LS and MLS deg. 0-1	LS deg. 2-3
No window	1.00	0.66
w/ Lanczos window	0.84*	0.74*
w/ von Hann window	0.78*	0.71*
w/ Blackman window	0.73*	0.67*
w/ Kaiser 50-dB window	0.84*	0.72*

* Valid for *N*>3 only. For N<3, values depend on *N* and are 10-40% lower

2.4 Impulse response and gain of commonly-used derivative filters

Here we briefly review a few commonly-used derivative filters. Except for the central difference filter, all filters considered here have the double function of smoothing and differentiating.

2.4.1 Central difference derivative filter

The simplest approximation of the derivative of a signal S at altitude $z(k)$ without a phase shift is the so-called *3-point central difference* which can be written:

$$S_f(k) = \frac{1}{2}\big(S(k+1) - S(k-1)\big)$$

(2.49)

Here we work in units of sampling bins rather than physical units, i.e., we assume the sampling resolution is δz=1. We recognize the set of coefficients:

$$c_n = \frac{n}{2} \qquad\qquad -1 \le n \le 1$$

(2.50)

The transfer function, obtained from **Eq. (2.49)** is:

$$\lambda(\omega) = \frac{1}{2}\left[-e^{-i\omega} + 0 + e^{i\omega}\right] = i\sin\omega$$

(2.51)

Following the notation of **Eq. (2.18)** (odd symmetry) and using the values of the coefficients c_n (**Eq. (2.50)**), we then compute the gain, i.e., the ratio of the value approximated by the central difference (**Eq. (2.51)**) to the value of the ideal derivative (**Eq. (2.17)**) and find:

$$G(f) = \frac{H(f)}{2\pi f} = \frac{\sum_{n=1}^{1}\frac{n}{2}\sin(2\pi n f)}{\pi f} = \frac{\sin 2\pi f}{2\pi f}$$

(2.52)

This equation shows that the central difference conserves the slope of the original signal for f=0 only, and underestimates this slope for all other frequencies. **Figure 2.9** shows the transfer function H (red solid curve) and gain G (blue solid curve) for the 3-point central differences.

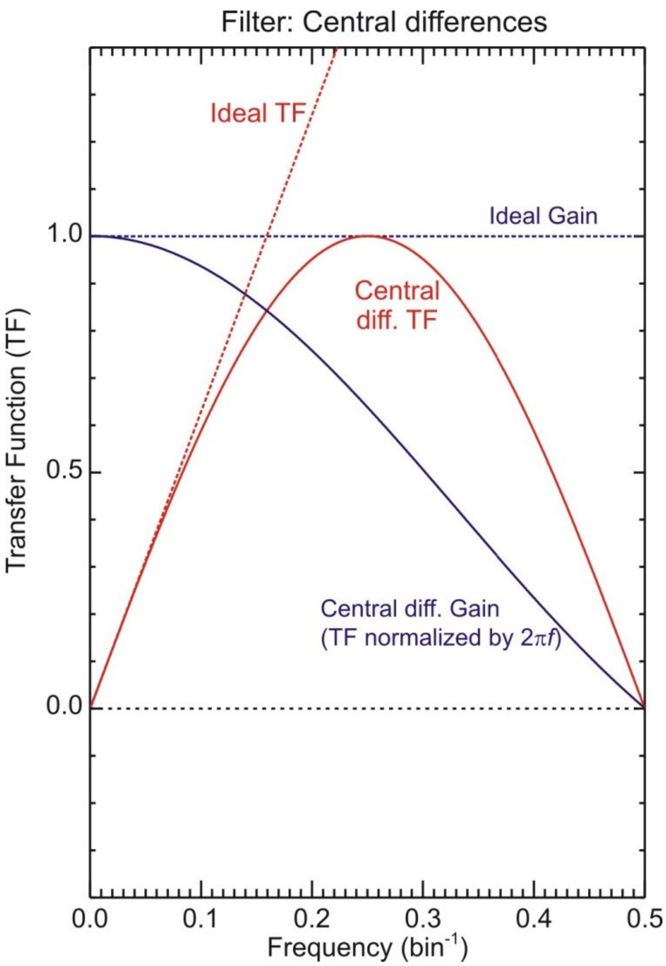

Figure 2.9 Transfer function and gain of the central difference digital filter. The gain (blue curve) is the transfer function (red curve) normalized by $2\pi f$, which is the real part of the ideal differentiator $i\omega$

Just like for the smoothing filters presented in **section 2.3**, we can design derivative low-pass filters that will conserve the slope of the signal for low values of frequency and attenuate the slope (or noise) for higher frequency values. A few examples are given below.

2.4.2 Least squares derivative filters (or Savitsky-Golay derivative filters)

In **paragraph 2.3.1**, we derived the coefficients of a 5-point boxcar function which was equivalent to fitting the signal using the least-squares technique with a polynomial of degree 1 (straight line). We can indeed use the second normal equation (second equation of the system of

Eqs. (2.20)) to compute c_1, which is the value of the slope of the fitting function. Applying Faulhaber's summing formula to a polynomial of degree 1 (Knuth, 1993), we find the values of the filter coefficients as a function of the total number of terms N_T to be:

$$c_n = \frac{12}{N_T\left(N_T^2-1\right)}n = \frac{3}{N(N+1)(2N+1)}n \qquad -N \le n \le N \text{ and } N_T = 2N+1 > 2$$

(2.53)

For $N_T = 2N+1 = 3$ points, that corresponds to the central difference:

$$c_n = \frac{n}{2} \qquad -1 \le n \le 1$$

(2.54)

For $N_T = 2N+1 = 5$ points, that corresponds to:

$$c_n = \frac{n}{10} \qquad -2 \le n \le 2$$

(2.55)

For $N_T = 2N+1 = 7$ points, that corresponds to:

$$c_n = \frac{n}{28} \qquad -3 \le n \le 3$$

(2.56)

Using a similar mathematical development, the filter coefficients corresponding to the least-squares fitting technique by higher order polynomials can also be obtained. For polynomials of degrees 3 and 4 (cubic and quartic) we have:

$$c_n = 225\frac{(3N_T^4-18N_T^2+31)n-28(3N_T^2-7)n^3}{N_T(N_T^2-1)(3N_T^4-39N_T^2+108)} \qquad -N \le n \le N \text{ and } N_T = 2N+1 > 3$$

(2.57)

For $N_T=2N+1=5$ points, that corresponds to:

$$c_n = \frac{455-119n^2}{504}n \qquad -2 \le n \le 2$$

(2.58)

For $N_T=2N+1=7$ points, that corresponds to:

$$c_n = \frac{397-49n^2}{1512}n \qquad -3 \le n \le 3$$

(2.59)

The coefficients of the smoothing and derivative filters associated with the least squares fitting by polynomials of degrees 1 through 6 are provided by Savitsky and Golay (1964) with corrected values in Steinier et al. (1972). The impulse response and gain of these filters are plotted in **Figure 2.10** for polynomials of degree 1 and 2 and **Figure 2.11** for polynomials of degree 3 and 4, and for full widths ranging between 3 and 25 points.

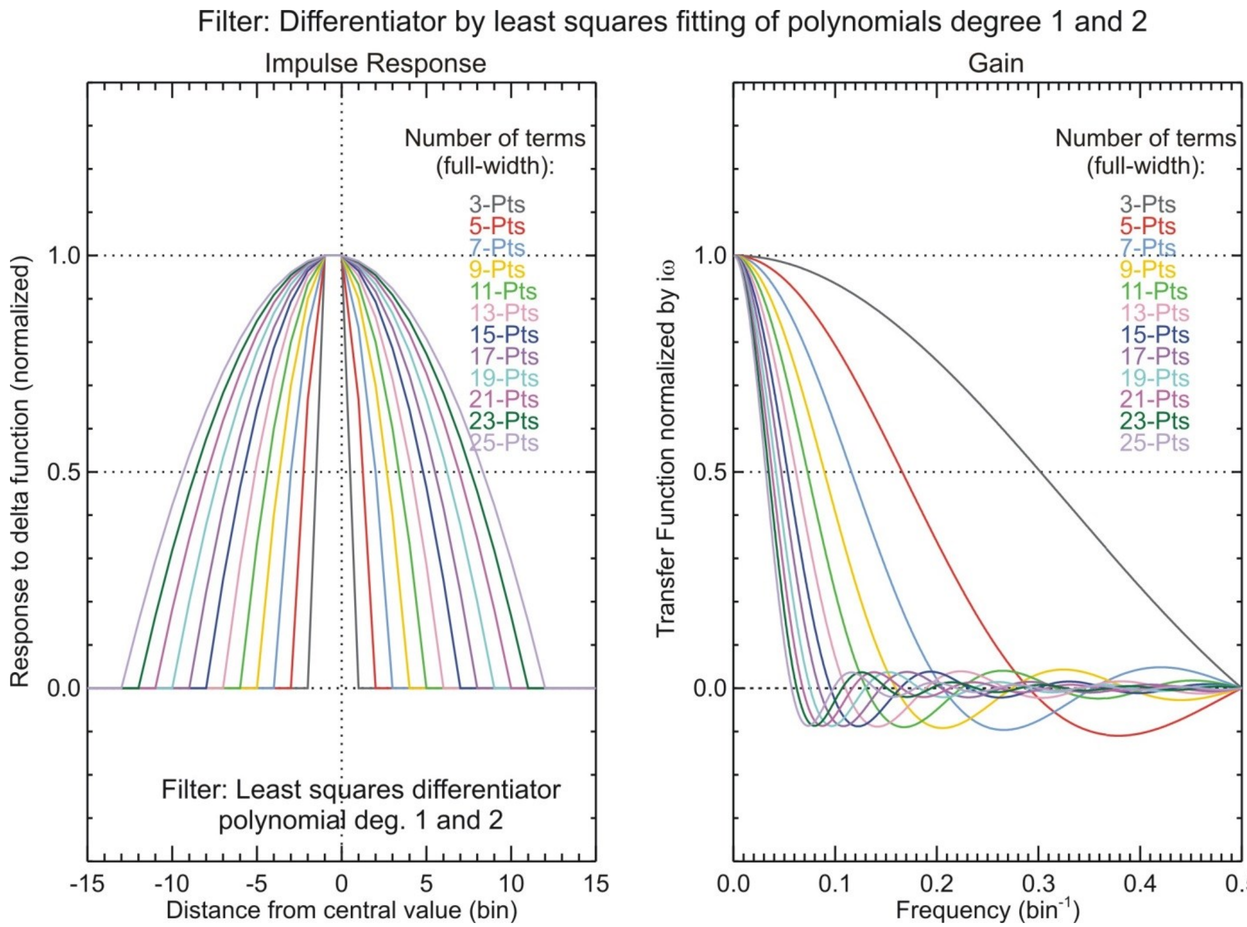

Figure 2.10 Impulse response (left) and gain (right) of derivative filters obtained from the calculated slope of a polynomial of degrees 1 and 2 using the least-squares fitting method over an interval comprising 2*N*+1 points (full width). The gain is the transfer function normalized by 2π*f*. Full widths range from 3 to 25 points

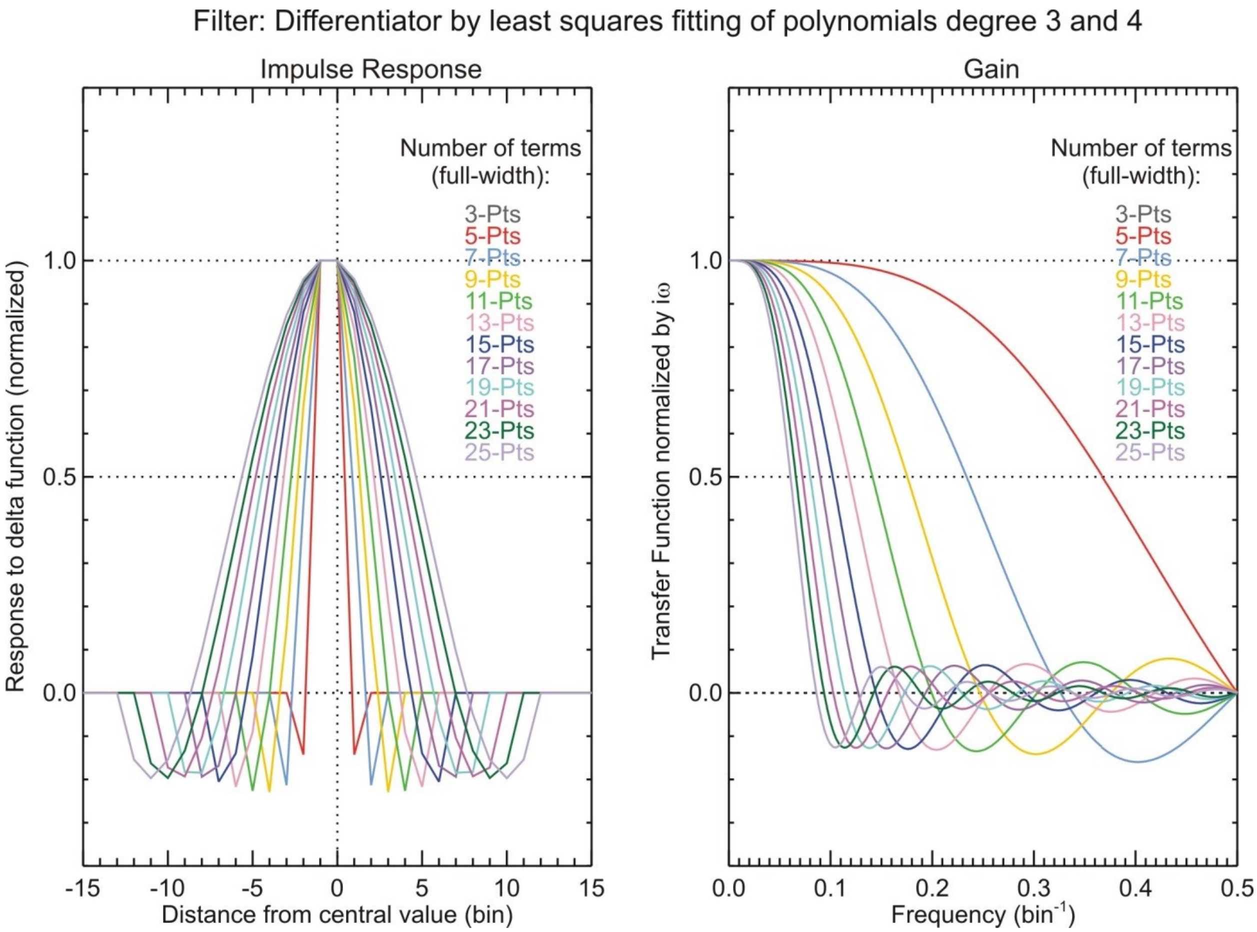

Figure 2.11 Same as Figure 2.10, but fitting with polynomials of degree 3 and 4 instead of 1 and 2

2.4.3 Low-pass derivative filters

Just as we did for the low-pass smoothing filters (**section 2.3.3**), we want to design a derivative low-pass filter with a prescribed cut-off frequency f_C. We therefore start with the initial conditions defining an ideal derivative low-pass filter:

$$H(f) = 2i\pi f \qquad \text{for } 0 < |f| < f_C$$

$$H(f) = 0 \qquad \text{for } f_C < |f| < 0.5$$

(2.60)

We find that these conditions are always true for a family of un-truncated Fourier series with the following transfer function:

$$H(f) = 2\sum_{n=1}^{\infty}\left(\frac{i}{n}\left(\frac{\sin(2\pi n f_C)}{\pi n} - 2 f_C \cos(2\pi n f_C)\right)\right)\sin(2\pi n f)$$

(2.61)

Again, we truncate the series to a finite number of terms at the expense of producing Gibbs ripples. The actual low-pass filter thus created has the following $2N+1$ coefficients and transfer function:

$$c_n = \frac{2f_C}{n}\left(\frac{\sin(2\pi n f_C)}{2\pi n f_C} - \cos(2\pi n f_C)\right) \qquad -N \le n \le N$$

$$H(f) = 2i\sum_{n=1}^{N}\left(\frac{f_C}{n}\left(\frac{\sin(2\pi n f_C)}{2\pi n f_C} - \cos(2\pi n f_C)\right)\right)\sin(2\pi n f)$$

(2.62)

2.4.4 Lanczos low-pass derivative filters

The low-pass filter coefficients will simply be multiplied by the sigma factors, as defined in **section 2.3**, to obtain the smooth derivative filter coefficients:

$$c_n = \frac{2f_C}{n}\left(\frac{\sin(2\pi n f_C)}{2\pi n f_C} - \cos(2\pi n f_C)\right)\frac{\sin(\pi n / N)}{\pi n / N} \qquad -N \le n \le N$$

(2.63)

2.4.5 Kaiser window and NERD filter

The low-pass filter coefficients are multiplied by the Kaiser window weights to obtain the coefficients of the Near-Equal-Ripple Derivative (NERD) filter:

$$c_n = \frac{2f_C}{n}\left(\frac{\sin(2\pi n f_C)}{2\pi n f_C} - \cos(2\pi n f_C)\right)\frac{I_0\left(\alpha\sqrt{1-(n/N)^2}\right)}{I_0(\alpha)} \qquad -N \le n \le N$$

(2.64)

Figure 2.12 shows the impulse response (left) and gain (right) of a low-pass derivative filter with f_C=0.2 before any convolution. **Figure 2.13** is similar to **Figure 2.12**, but after convolution by a Lanczos window. **Figure 2.14** is similar to **Figure 2.12**, but after convolution by a Kaiser window (50-dB attenuation). These figures show that the filters and the windows used are not optimized for all values of N. Therefore, the choice of filter must be carefully made together with the number of filter coefficients used.

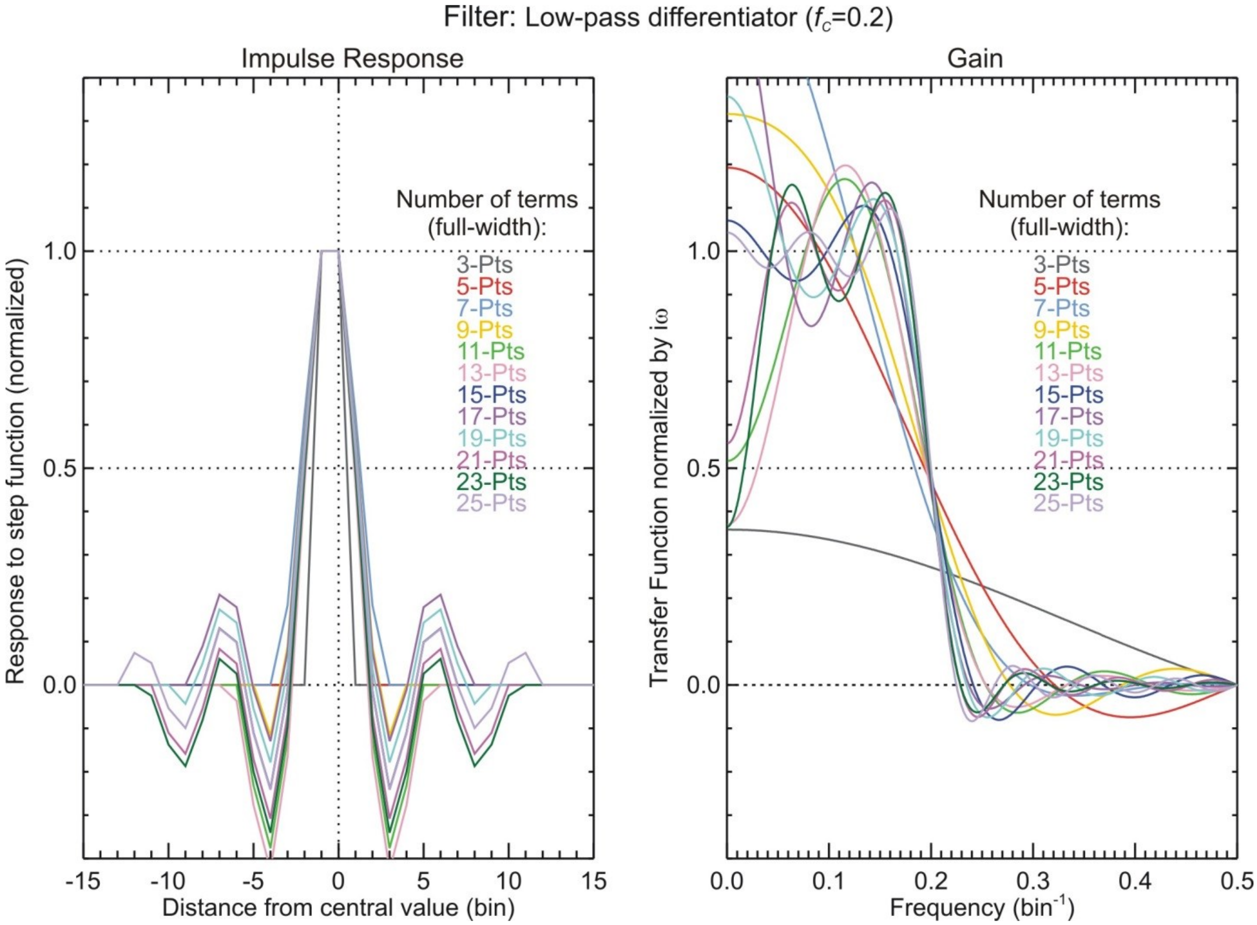

Figure 2.12 Impulse response (left) and gain (right) of a low-pass derivative filter (f_C=0.2). The gain is the transfer functions normalized by 2π*f*. Full widths range from 3 to 25 points

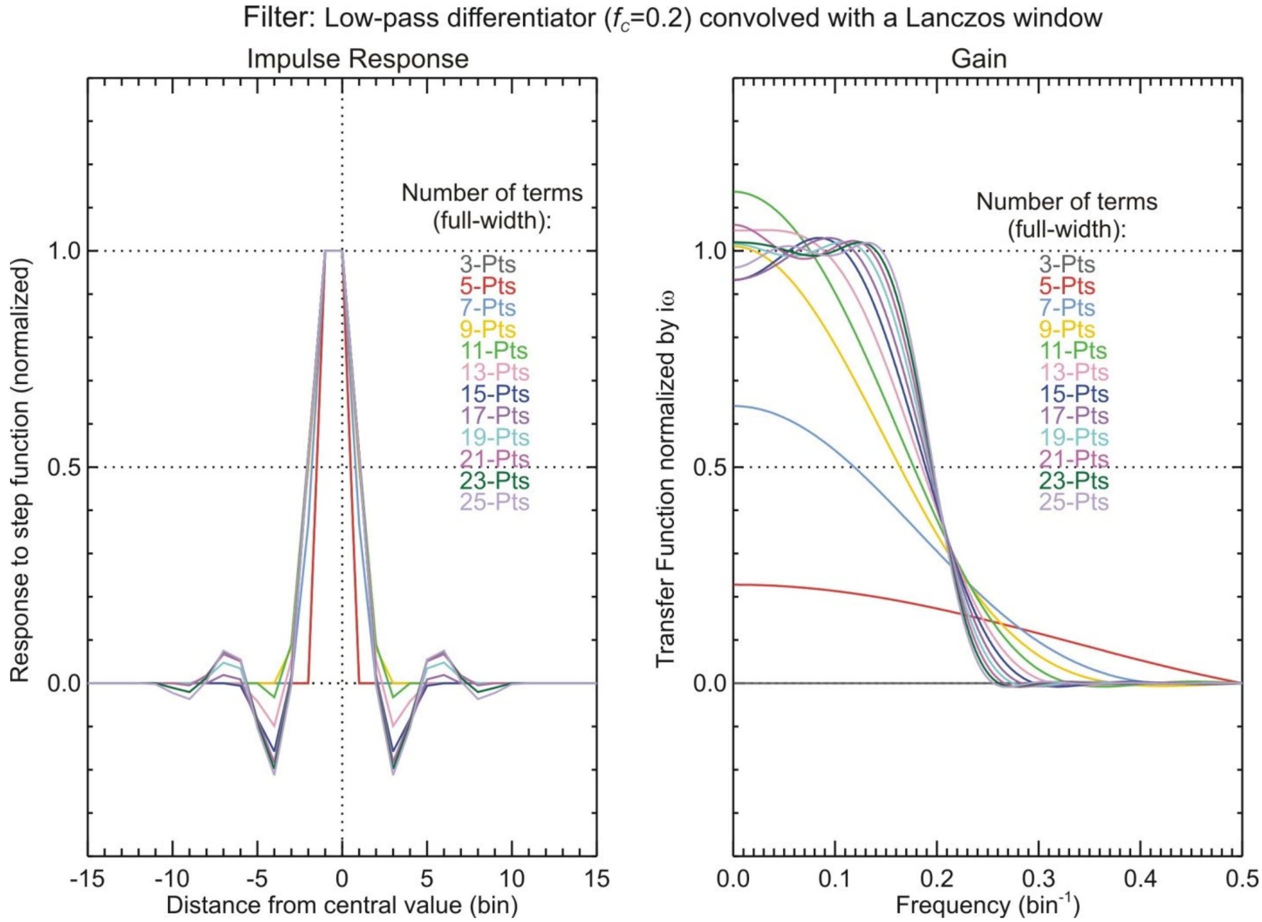

Figure 2.13 Same as Figure 2.12 but after convolution by a Lanczos window

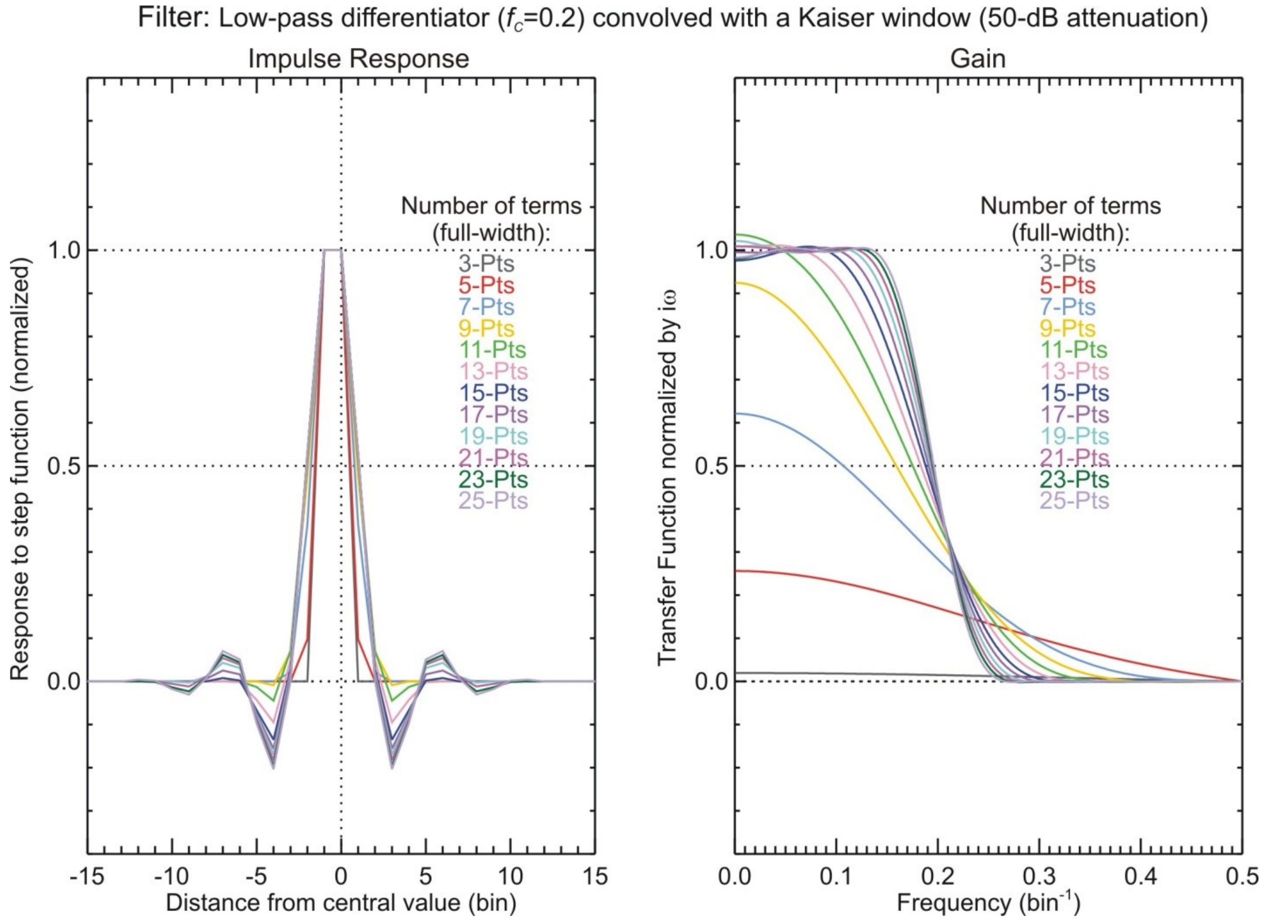

Figure 2.14 Same as but after convolution by a Kaiser window tuned for a 50-dB attenuation

3 Review of vertical resolution definitions used by NDACC lidar investigators

The filtering schemes or methods of several NDACC lidar investigators have been reviewed and compared in previous works, for e.g., Beyerle and McDermid (1999) and Godin et al., (1999). These studies concluded that vertical resolution was not consistently reported between the various investigators. Here we briefly review the filtering schemes or methods used by various NDACC lidar investigators, and how vertical resolution is reported in their data files as of 2011. This review provided critical input to the ISSI Team to determine which definitions of vertical resolution is appropriate for use in a standardized way across the entire network (see **section 4**).

In the case of the Observatoire de Haute-Provence (OHP) stratospheric ozone differential absorption lidar, a 2nd degree polynomial derivative filter (Savitsky-Golay derivative filter) is used. Vertical resolution is reported following a definition based on the cut-off frequency of the digital filter (Godin-Beekmann et al., 2003).

For the JPL stratospheric ozone and temperature lidars at Table Mountain, CA and Mauna Loa, Hawaii, filtering is done by applying a 4th degree polynomial least-squares fit (Savitsky-Golay derivative filter) to the logarithm of the signals for ozone retrieval. For the temperature profiles, a Kaiser filter is applied to the logarithm of the relative density profile. In both ozone and temperature cases, the cutoff frequency of the filter, reversed to the physical domain, is reported as vertical resolution (Leblanc et al., 2012).

The NASA-GSFC ozone DIAL algorithm (STROZ instrument) (Beyerle and McDermid, 1999) uses a least-squares 4^{th} degree polynomial fit derivative filter (Savitsky-Golay derivative filter). The definition of vertical resolution in the NDACC-archived data files is based on the impulse response of a delta function, by measuring the FWHM of the filter's response. As shown in **section 4**, there is a linear relation between the FWHM and the width of the window (number of points) used. For the temperature retrieval (Gross et al., 1997), the profiles are smoothed using a low-pass filter (Kaiser and Reed, 1977), and a simple ad hoc step function is used to define the values of the vertical resolution.

For the RIVM ozone lidar located in Lauder, New Zealand (Swart et al., 1994), the definition of vertical resolution is based on the width of the fitting window used for the ozone derivation.

The tropospheric ozone DIAL at Reunion Island (France) uses a 2^{nd} degree polynomial least-squares fit (Savitsky-Golay derivative filter) to filter the ozone measurements. The vertical resolution is reported as the cut-off frequency of the corresponding digital filter (same ozone retrieval as for the OHP lidar). For the temperature profiles using the Rayleigh backscatter lidar measurements at Reunion Island, a Hamming filter is applied on the temperature profile. The width of the window used is reported as the vertical resolution.

For climatology studies, the PCL temperature algorithm applies a combination of smoothing by 3s and 5s filters or a Kaiser filter on the temperature profiles (e.g. Argall and Sica, 2007). Similar filters are used in space or time for spectral analysis of atmospheric waves (e.g. Sica and Russell 1999). Filter parameters are reported in the data files locally produced and distributed to the scientific user community. Previously files were distributed to users with the type of filter and full bandwidth of the filter. The variance reduction of the filter is folded into the random uncertainties provided. The product of the data spacing and the filter bandwidth gives the full influence of the filter at each point. With the development of a temperature retrieval algorithm based on an optimal estimation method, vertical resolution of the temperature profile is now available as a function of altitude (Sica and Haefele 2015).

The ozone DIAL and temperature algorithms of the NDACC lidar in Tsukuba, Japan uses 2^{nd} and 4^{th} degree polynomial least-squares fits (Savitsky-Golay derivative filter). The vertical resolution is calculated from a simulation model that determines the FWHM of the impulse response to an ozone delta function. The FWHM is then mapped as a function of altitude. For temperature a von Hann (or Hanning) window is used on the logarithm of the signal (B. Tatarov, personal communication, 2010).

The IFU tropospheric ozone DIAL algorithm (instrument located in Garmisch-Partenkirchen, Germany) uses least-squares first and third degree polynomial fits, as well as a combination of a linear fit and a Blackman-type window (Eisele and Trickl, 2005; Trickl, 2010). These filters have a reasonably high cut-off frequency and do not transmit as much noise as the derivative filters used earlier at IFU (Kempfer et al., 1994). To report vertical resolution in the data files, a Germany-based standard definition of vertical resolution is used, following the Verein Deutscher Ingenieure DIAL guideline VDI-4210 published in 1999 (VDI, 1999). This definition is based on the impulse response to a Heaviside step function. The vertical resolution is given as the distance separating the positions of the 25% and 75% in the rise of the response, which is approximately equivalent to the FWHM of the response to a delta function. In the case of the ozone DIAL the vertical resolution of both the Blackman-type filter used and the combined least-squares-derivative plus Blackman filter. A vertical resolution of 19.2 % or 19.6 % of the filtering interval was determined, respectively. For small intervals the latter value may change, i.e., the least-squares fit for determining the derivative is executed over just a few data points. For comparison, an arithmetic average yields a vertical resolution of 50 % of the filtering interval.

Having reviewed the vertical resolution definitions and schemes used across NDACC and elsewhere, three definitions or approaches can be clearly identified. The first definition is the number of filter coefficients used, the second definition is based on the cut-off frequency of the filter, and the third definition is based on the width of the impulse response of the filter. Those definitions were already mentioned by Beyerle and McDermid (1999), but no decision was made within NDACC to find a standardized approach across the network. **Section 2** showed that not all filters have the same properties, and that the characteristics of a filter do not simply depend on the number of coefficients used, but instead on a combination of the number of coefficients and their values. Indeed **Figure 3.1** below shows the gain of several filters having the same number of coefficients (5-pts for the smoothing filters on the left hand plot, and 7-pts for the derivative filters on the right hand plot). It is obvious that, depending on the filter and/or window used, the transition region between pass-band and stop-band is located at very different frequencies. In the examples shown, it is located between f=0.12 and f=0.35 for smoothing filters, while the derivative filters show considerably more variability.

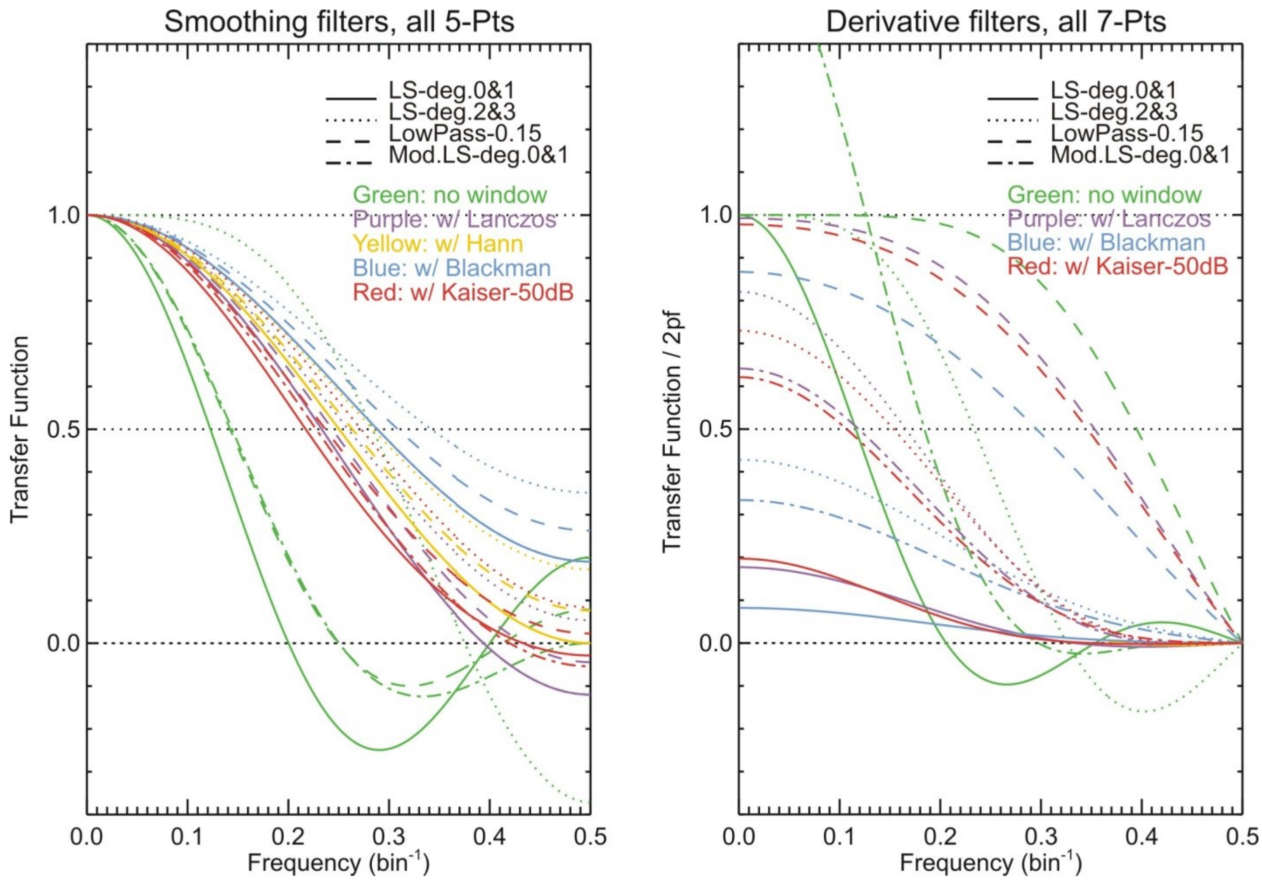

Figure 3.1 Gain of several smoothing (left) and derivative (right) filters, all having the exact same number of coefficients 2*N*+1 (5-pts full-width for the smoothing filters and 7-pts full-width for the derivative filters)

Finding transition regions at different frequencies means that the smoothing effect of the filters on the signal is different even though the number of coefficients is the same. A vertical resolution definition based on the number of coefficients is therefore not reliable. Instead we need to choose a standardized definition based on objective parameters that are directly related to the effect a filter has on the signal. Two such definitions are proposed thereafter, definitions that are similar or closely related to the two remaining definitions identified in this **section**.

4 Proposed standardized vertical resolution definitions for the NDACC lidars

The two definitions proposed in this report were chosen because they provide a straightforward characterization of the underlying smoothing effect of filters (see **section 2**), and they appear to be already used by a large number of NDACC investigators (see **section 3**). The first definition is based on the width of the impulse response of the filter. The second definition is based on the cut-off frequency of the filter. Further justification for the choice of either definition is provided at the end of this section.

4.1 Definition based on the FWHM of a finite impulse response

The full-width-at-half-maximum (FWHM) of an impulse response, as introduced in **section 2**, is computed by measuring the distance (in bins) between the two points at which the response magnitude falls below half of its maximum amplitude. The NDACC-lidar-standardized definition of vertical resolution proposed here is computed from the response I_{OUT} of a Kronecker delta function for smoothing filters, and a Heaviside step function for derivative filters. Because of the dynamic range of the lidar signals (or ozone or temperature profiles), we assume that the number of filter coefficients varies with altitude. Therefore, the standardized vertical resolution is estimated separately for each altitude $z(k)$, and the procedure can be summarized as follows:

1) Define and/or identify the $2N(k)+1$ filter coefficients $c(k,n)$ used to perform the smoothing or differentiation operation on the lidar signal (or the ozone or temperature profile):

$$S_f(k) = \sum_{n=-N(k)}^{N(k)} c(k,n)S(k+n) \qquad \text{for } N(k) < k < nk - N(k) \tag{4.1}$$

2) Construct an impulse function of finite length $2M(k)+1$ to be convolved with the filter coefficients. The value of $M(k)$ is not critical but has to be greater or equal to $N(k)$. For smoothing filters, the impulse function is the Kronecker delta function which can be written:

$$I_{INP}(k,m) = \delta_0(m) \quad \text{with} \quad -M(k) \le m \le M(k) \quad \text{and} \quad N(k) \le M(k) \le \frac{nk-1}{2} \tag{4.2}$$

This function equals 1 at the central point (m=0) and equals 0 everywhere else. For derivative filters, the impulse function is the Heaviside step function which can be written:

$$I_{INP}(k,m) = H_S(m) \quad \text{with} \quad -M(k) \le m \le M(k) \quad \text{and} \quad N(k) \le M(k) \le \frac{nk-1}{2} \tag{4.3}$$

This function equals 0 at all locations below the central point (m<0) and equals 1 everywhere else.

3) Convolve the filter coefficients with the impulse function in order to obtain the impulse response I_{OUT}:

$$I_{OUT}(k,m) = \sum_{n=-N(k)}^{N(k)} c(k,n) I_{INP}(k,m+n)$$

(4.4)

4) Estimate the full width at half-maximum (FWHM) of the impulse response I_{OUT}, by measuring the distance Δm_{IR}, in bins, between the two points (located on each side of the central bin) where the response magnitude falls below half of the maximum amplitude:

$$I_{OUT}(k,m_1(k)) = 0.5\max\left(I_{OUT}(k,m_i)\right) \qquad \text{for all } -M(k) \le m_i \le 0$$

$$I_{OUT}(k,m_2(k)) = 0.5\max\left(I_{OUT}(k,m_i)\right) \qquad \text{for all } 0 \le m_i \le M(K)$$

$$\Delta m_{IR}(k) = \left| m_1(k) - m_2(k) \right|$$

(4.5)

For a successful identification of the FWHM, the impulse response should have only two points where its value falls below half of its maximum amplitude, which is normally the case for all smoothing and derivative filters used within their prescribed domain of validity (see examples in **section 2**). In the event that more than two points exist, the two points farthest from the central bin should be chosen in order to yield the most conservative estimate of vertical resolution.

5) Compute the standardized vertical definition Δz_{IR} as the product of the lidar sampling resolution δz and the estimated FWHM:

$$\Delta z_{IR}(k) = \delta z \Delta m_{IR}(k)$$

(4.6)

Figure 4.1 summarizes the estimation procedure just described. The unsmoothed signal yields a FWHM of 1 bin. This result is easily derived by considering null coefficients everywhere except at the central point (m=0), where the coefficient equals 1. The intercept theorem within the triangles formed by the impulse response at the central point and its two adjacent points (m=-1 and m=1) yields a FWHM of 1 bin, and the standardized vertical resolution using the present impulse response-based definition will always be greater or equal to the sampling resolution:

$$\Delta z_{IR}(k) \ge \delta z \quad \text{for all } k$$

(4.7)

When several filters are applied successively to the signal, the response of the filter must be computed each time a filtering operation occurs, and vertical resolution needs to be computed only after the last filtering occurrence. The process can be summarized as follows: a first impulse response is computed with the first filtering operation. If no further filtering occurs, the impulse response is used to determine the FWHM and vertical resolution. If a second filtering operation occurs, the impulse response is used as input signal, and a second response is computed from the convolution of this input signal with the coefficients of the second filter. If no further filtering occurs, the second response is used to determine the FWHM and vertical resolution. If a third filtering operation occurs, the response output from the second convolution is used as input signal of the third convolution, and so on until no more filtering occurs. Vertical resolution is always computed from the final output response, i.e., after the final filtering operation. The schematics shown in **Figure 4.2** summarize the procedure.

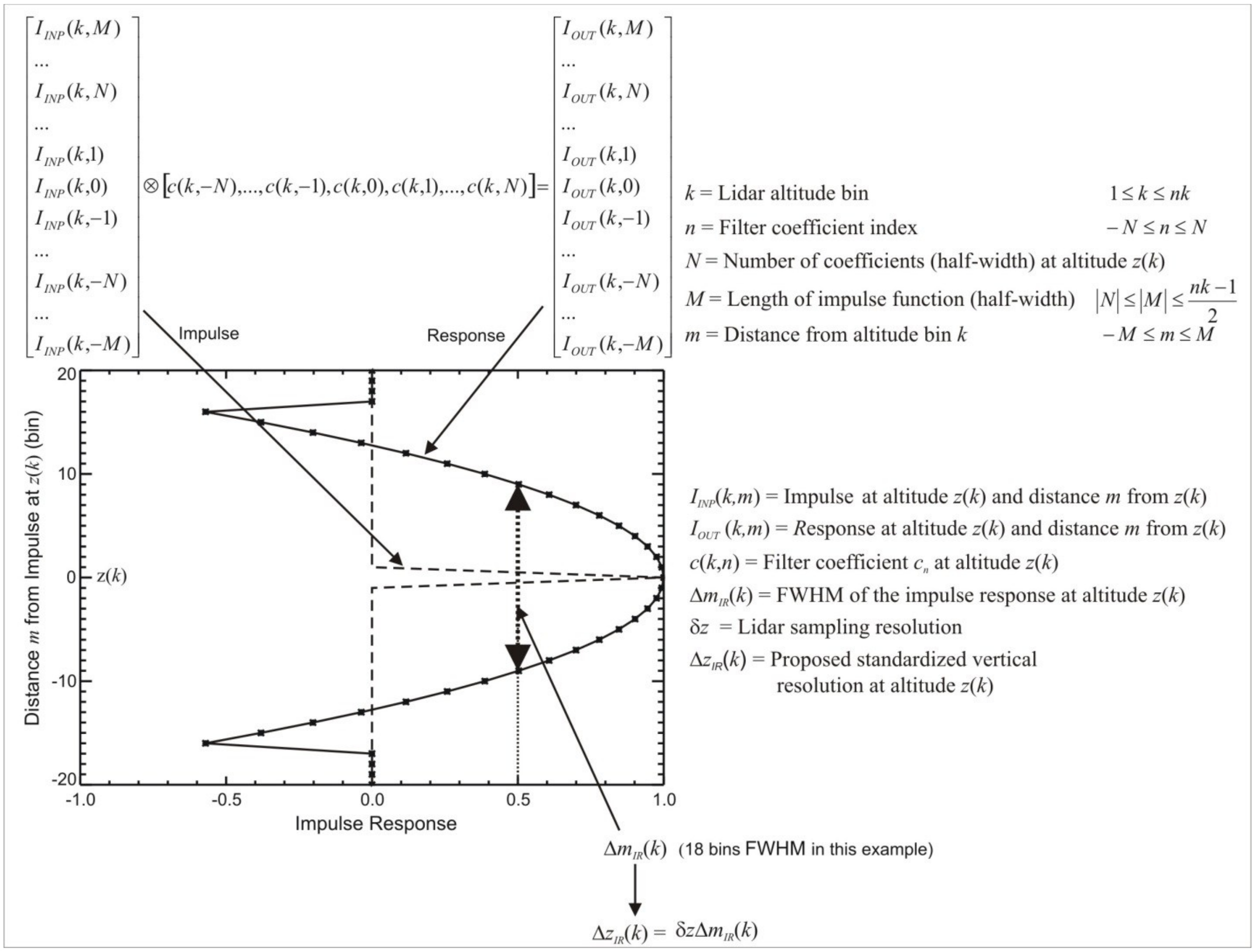

Figure 4.1 Schematics summarizing the procedure to follow to compute the standardized vertical resolution with a definition based on the impulse response FWHM Δz_{IR}

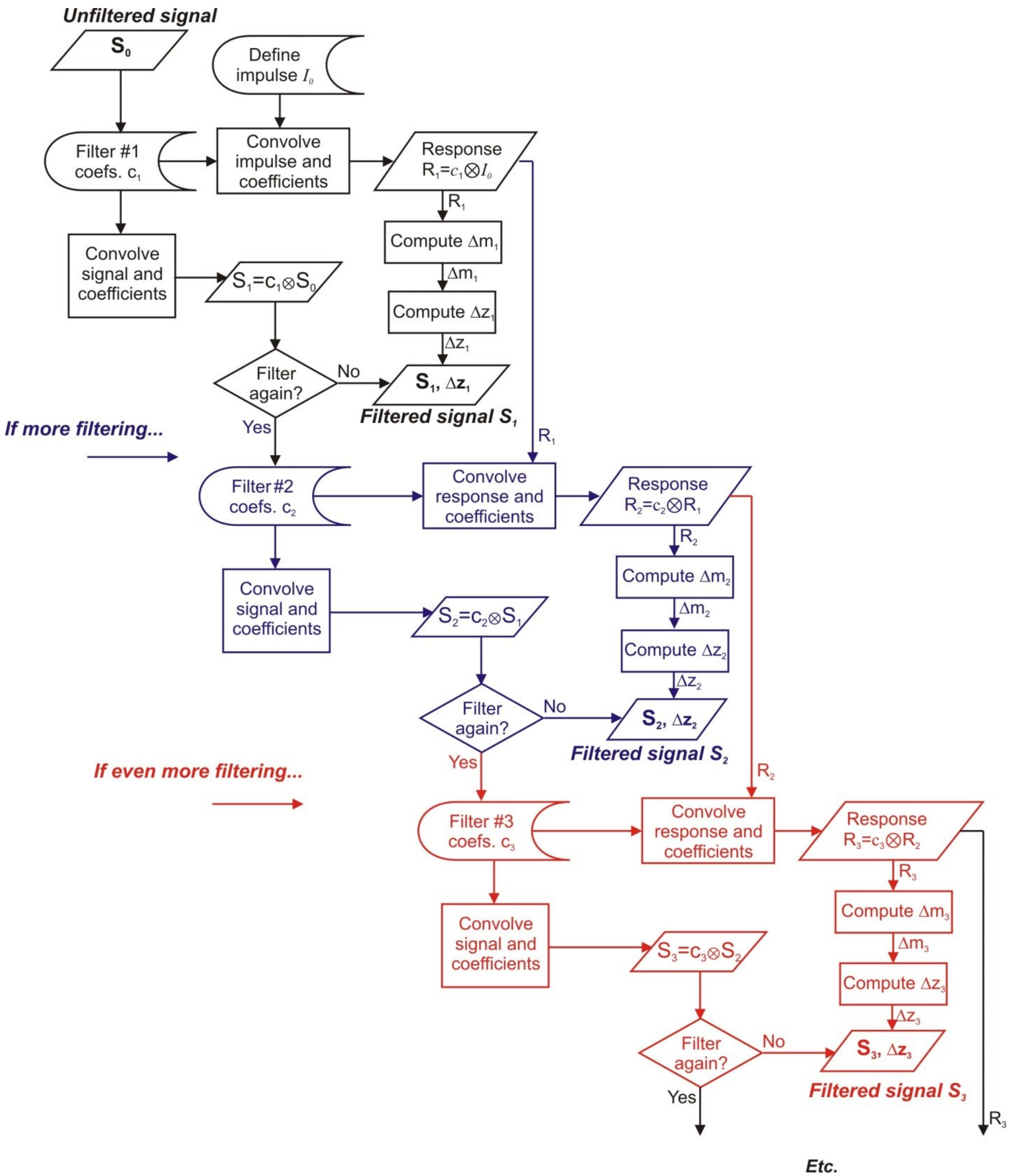

Figure 4.2 Schematics summarizing the procedure to follow to compute the standardized vertical resolution with a definition based on impulse response when the signal or profile is filtered multiple times

4.2 Definition based on the cut-off frequency of digital filters

The cut-off frequency of digital filters is defined as the frequency at which the value of the filter's gain is 0.5, typically located at the center of the transition region between the passband and the stopband (see **section 2**). The NDACC-lidar-standardized definition proposed here is computed from the cut-off frequency f_C, which is determined from the gain of the filter obtained by applying a Laplace Transform to the coefficients of the filter used. Once again, because of the dynamic range of the lidar signals, filtering a lidar signal (or ozone/temperature profile) typically requires to use a number of filter coefficients varying with altitude. Starting with a lidar signal (or ozone or temperature profile) S made of nk equally-spaced elements in the vertical dimension, the standardized vertical resolution is estimated separately for each altitude $z(k)$, and the procedure can be summarized as follows for each altitude considered:

1) Define and/or identify the $2N(k)+1$ filter coefficients $c(k,n)$ used to perform the smoothing or differentiation operation on the lidar signal (or on the ozone or temperature profile):

$$S_f(k) = \sum_{n=-N(k)}^{N(k)} c(k,n) S(k+n) \qquad \text{for } N(k) < k < nk - N(k) \tag{4.8}$$

2) Apply the Laplace Transform to the coefficients to determine the filter's transfer function and gain. For non-derivative smoothing filters, the coefficients have even symmetry, i.e., $c(k,n)=c(k,-n)$, and the gain is written:

$$G(k,f) = H(k,f) = c(k,0) + 2\sum_{n=1}^{N(k)} c(k,n)\cos(2\pi nf) \qquad 0 < f < 0.5 \tag{4.9}$$

For derivative filters, the coefficients have odd symmetry, i.e., $c(k,n)=-c(k,-n)$, and if δz is the sampling resolution, the gain can be written:

$$G(k,f) = \frac{H(k,f)}{2\pi f} = 2\sum_{n=1}^{N(k)} c(k,n)\frac{\sin(2\pi nf)}{2\pi f} \qquad 0 < f < 0.5 \tag{4.10}$$

For a successful cut-off frequency estimation process, the gain must be computed with normalized coefficients c_n, that is, the coefficients must meet the following normalization condition:

$$\sum_{n=-N(k)}^{N(k)} c(k,n) = 1 \qquad \text{for smoothing filters}$$

$$2\sum_{n=1}^{N(k)} n c(k,n) = 1 \qquad \text{for derivative filters} \tag{4.11}$$

3) Estimate the cut-off frequency, i.e., the frequency f_C at which the gain equals 0.5:

$$G\left(k, f_C(k)\right) = 0.5 \qquad 0 < f_C(k) \le 0.5 \tag{4.12}$$

For a successful identification, the gain should have only one crossing with the 0.5-line. This is normally the case for all smoothing and derivative filters used within their prescribed domain of validity. In the event that several crossings exist, the frequency closest to zero should be chosen to ensure that the most conservative estimate of vertical resolution is kept.

4) Calculate the cut-off length Δm_{FC} (unit: bins), i.e., the inverse of the frequency f_C normalized to the sampling width:

$$\Delta m_{FC}(k) = \frac{1}{2 f_C(k)} \tag{4.13}$$

5) Compute the standardized vertical definition Δz_{FC} as the product of the lidar sampling resolution δz and the cut-off length Δm_{FC} at that altitude:

$$\Delta z_{FC}(k) = \delta z \Delta m_{FC}(k) = \frac{\delta z}{2 f_C(k)} \tag{4.14}$$

Figure 4.3 summarizes the estimation procedure just described. The factor of 2 present in the denominator of **Eq. (4.13)** is usually not used in spectral analysis, when it is normally assumed that the minimum vertical scale that can be resolved by the instrument is twice the sampling resolution (Nyquist criterion). However, it is included here in order to harmonize the numerical values with the values computed using the impulse response definition. Using the present proposed definition, an unsmoothed signal yields a vertical resolution of δz and the standardized vertical resolution will always be at least equal to the sampling resolution:

$$\Delta z_{FC}(k) \geq \delta z \qquad \text{for all } k \tag{4.15}$$

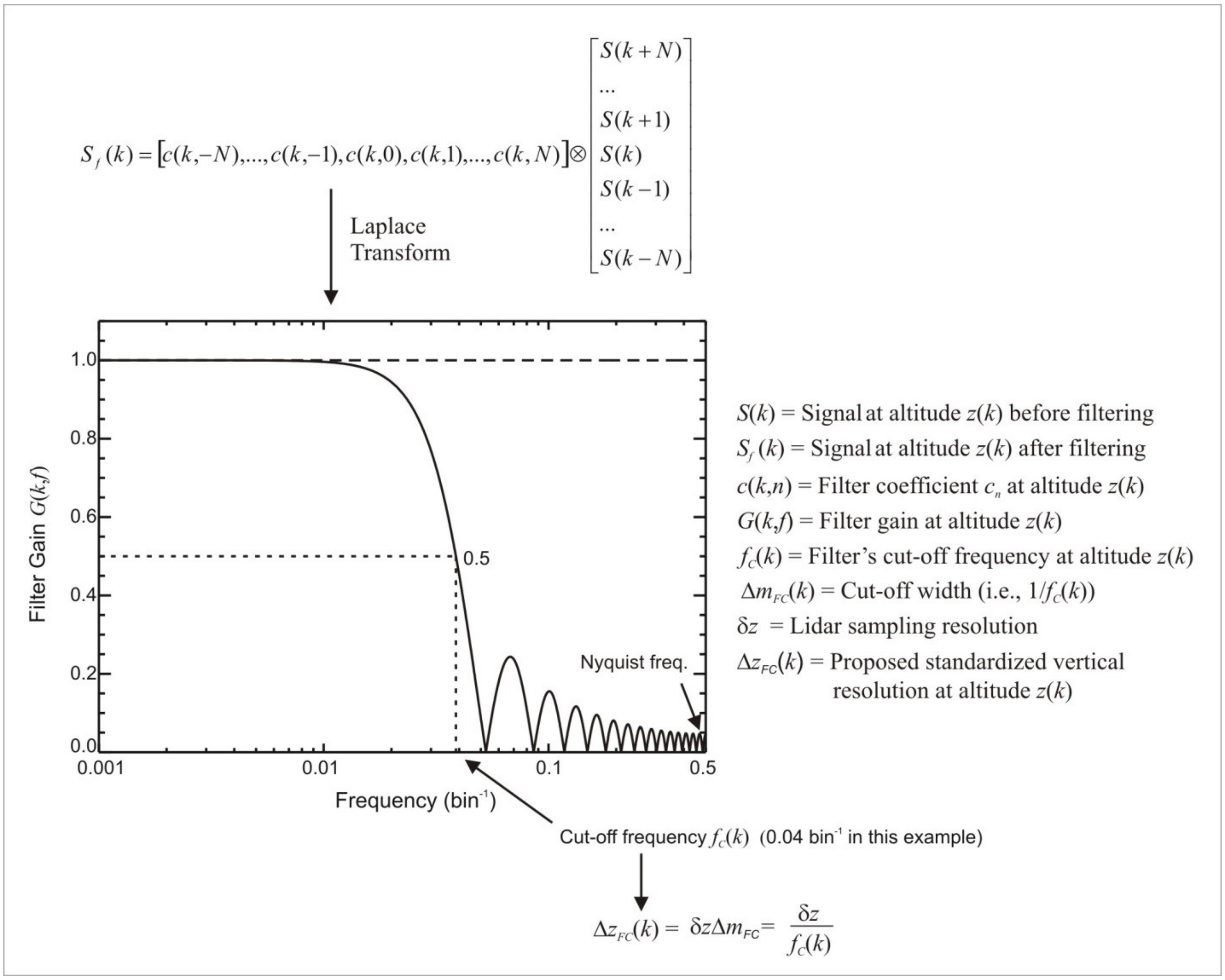

Figure 4.3 Schematics summarizing the procedure to follow to compute the standardized vertical resolution with a definition based on cut-off frequency Δz_{FC}

When several filters are applied successively to the signal, the transfer function must be computed each time a filtering operation occurs, but vertical resolution needs to be computed only after the last filtering occurrence. The process can be summarized as follows: a first transfer function (or gain) is computed with the first filtering operation. When the second filtering operation occurs, the gain computed using the coefficients of the second operation is multiplied by the gain computed during the first filtering operation. If no further filtering occurs, the result of this product is the gain that should be used to determine the cut-off frequency and vertical resolution. If a third filtering operation occurs, the product of the first and second gain must be multiplied by the third gain, and so on until no more filtering occurs. When the final filtering operation is reached, vertical resolution can be computed from the final output gain. The schematics shown in **Figure 4.4** summarize the procedure.

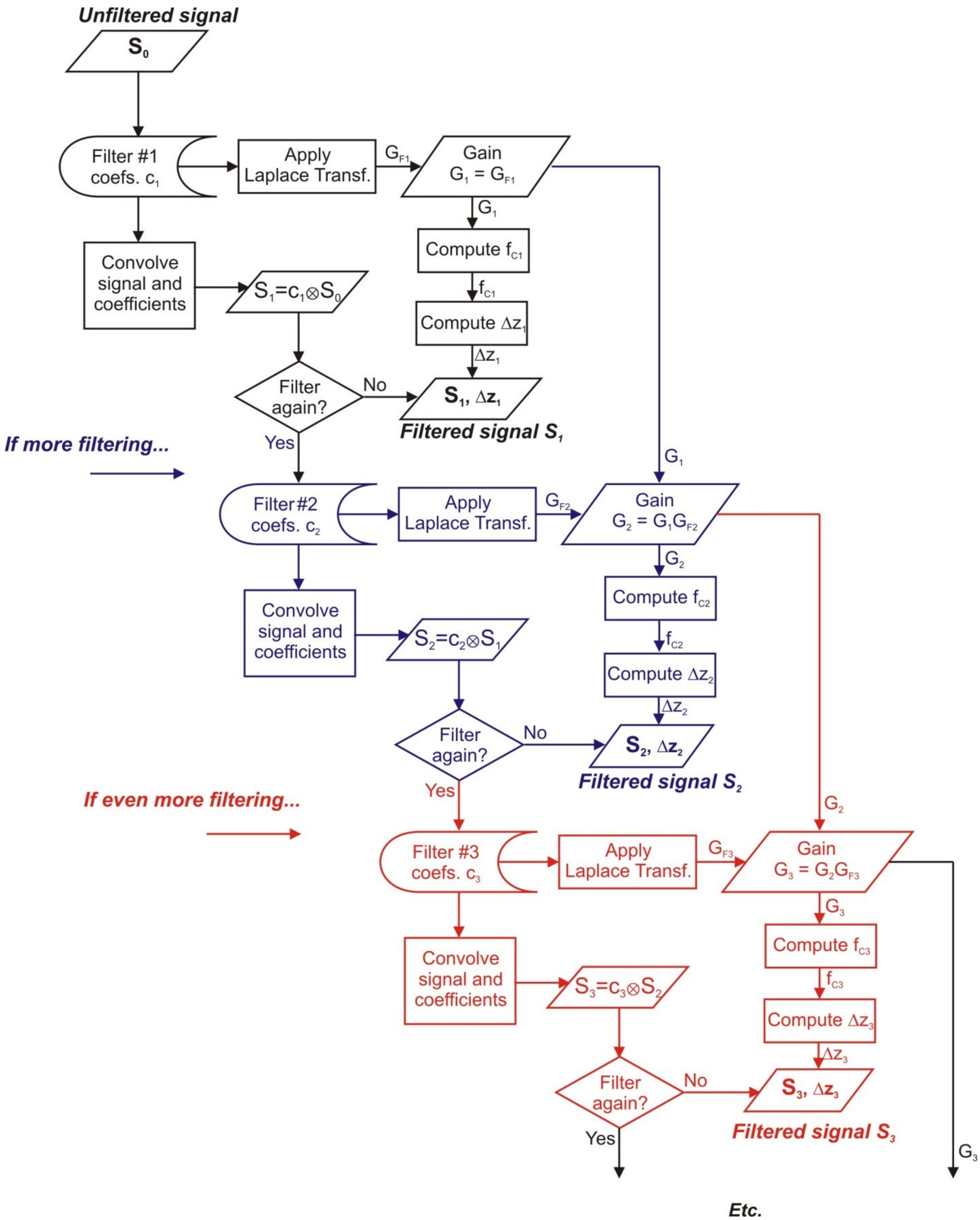

Figure 4.4 Schematics summarizing the procedure to follow to compute the standardized vertical resolution with a definition based on cut-off frequency when the signal or profile is filtered multiple times

4.3 Comparison between the impulse response-based and cut-off frequency-based definitions

In **sections 4.1 and 4.2**, we showed that, when using the proposed definitions based on impulse response and cut-off frequency, the standardized vertical resolution of an unsmoothed lidar signal (or profile) is equal to the lidar sampling resolution. However this equality between the two definitions is not perfect for all filters. Here, we show that for most filters, there is a well-defined proportionality relation between the two definitions, but we also show that the proportionality factor depends on the type of filter used. In the rest of this section, for convenience we will work with vertical resolutions normalized by the sampling resolution (unit: bins). The results are therefore shown as cut-off width Δm_{FC} and impulse response FWHM Δm_{IR} instead of Δz_{FC} and Δz_{IR} respectively, which is equivalent to assuming δz=1.

Figure 4.5 shows, for the smoothing filters introduced in **section 2**, the correspondence between the standardized vertical resolutions (in bins) computed using the cut-off frequency and using the impulse response, for full-widths comprised between 3 and 25 points. The black solid circle at coordinate (2,1) indicates the vertical resolution for the unsmoothed signal (or profile). The grey horizontal and vertical dash-dotted lines indicate the highest possible vertical resolutions for the impulse response-based and cut-off frequency-based definitions respectively. The grey dotted straight lines indicate the result of the linear regression fits between the two definitions, and the numbers at their extremity are the values of the slope for three of the four types of filters used. There is no proportionality between the two definitions for the low-pass filters (diamonds) because the cut-off frequency is prescribed for this type of filter. Note that the factors of 1.2 and 1.39 do not correspond to the ratio of 1.0 that is assumed for the unsmoothed signal. Very similar conclusions can be drawn for the derivative filters, as demonstrated by **Figure 4.6** (which is similar to **Figure 4.5** but for the derivative filters introduced in **section 2**).

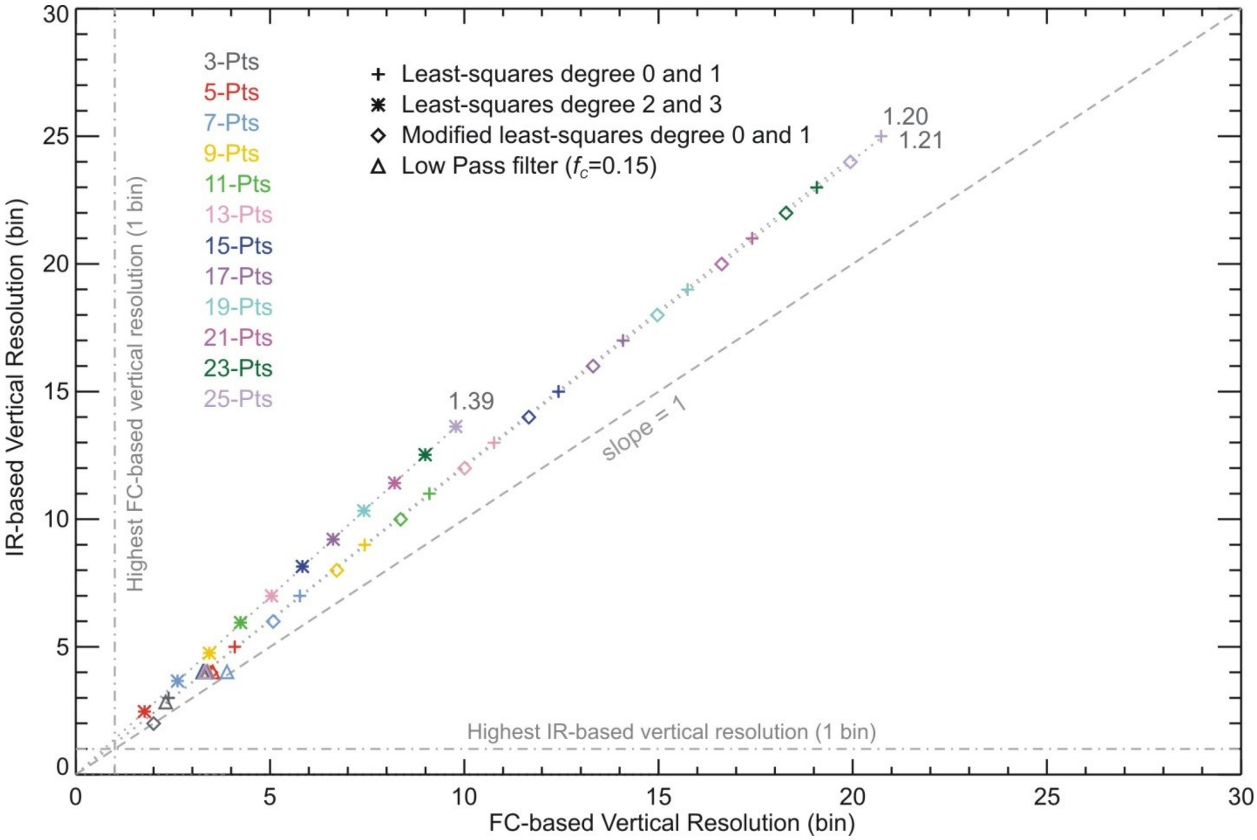

Figure 4.5 Comparison between the cut-off frequency-based and the impulse response-based standardized vertical resolutions for several smoothing filters introduced in section 2. The numbers at the end of the dotted straight lines indicate the proportionality constant (slope) between the 2 definitions for three of the four types of filters used. There is no such proportionality for the low-pass filter (prescribed cut-off frequency)

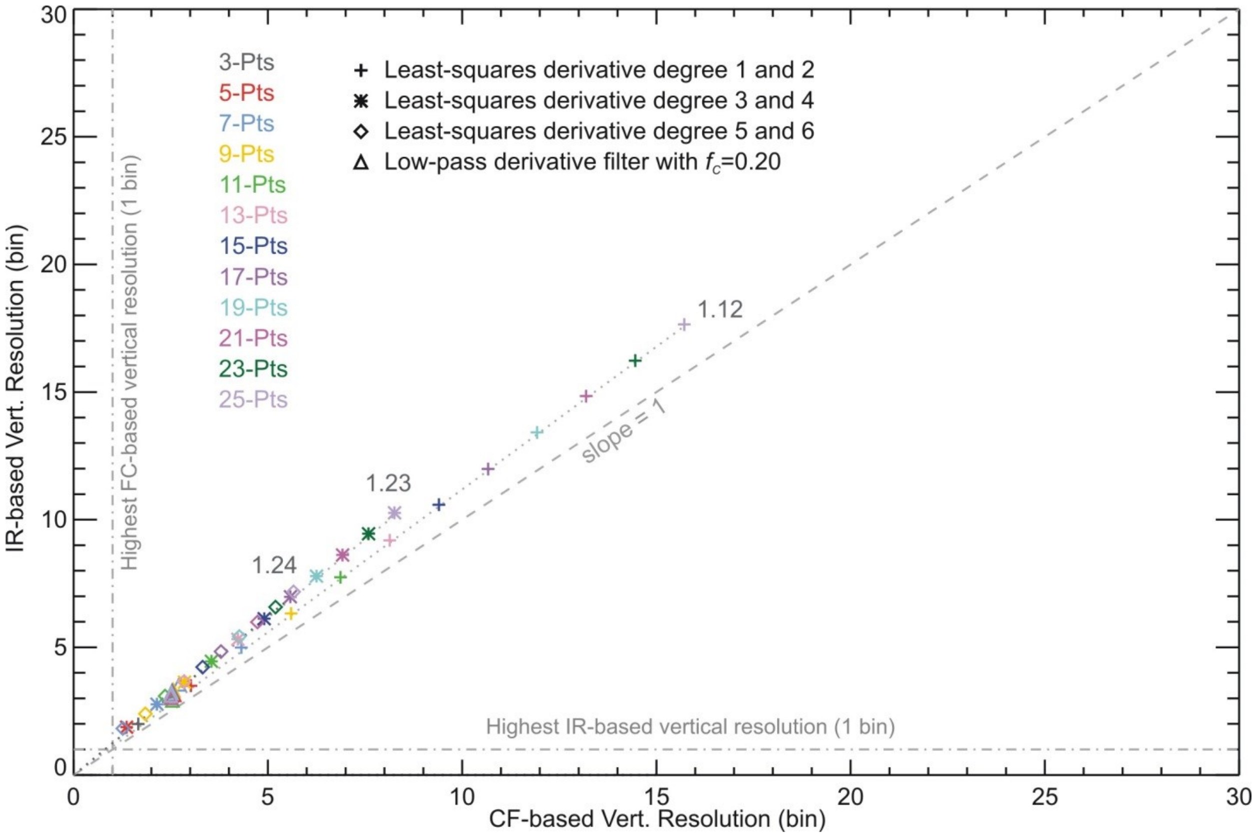

Figure 4.6 Same as Figure 4.5, but for derivative filters

Figure 4.7 is similar to **Figure 4.5**, but this time after the filters were convolved with the windows introduced in **section 2**. The windows change the proportionality constant between the two definitions, but this constant appears to be approximately the same for a given window, specifically around 1.04 for Lanczos, 1.0 for von Hann, 0.92 for Blackman, and 1.0 for Kaiser (50-dB). **Table 4.1** summarizes the proportionality constants for all filters and all windows introduced in **section 2**.

Table 4.1 Proportionality factor between the impulse response-based and the cut-off frequency-based definitions of vertical resolution for the filters and windows introduced in section 2

Ratio $\Delta z_{IR}/\Delta z_{FC}$	LS and MLS deg. 0-1	LS deg. 2-3	LS deriv. deg. 1-2	LS deriv. deg. 3-4	LS derive. deg. 5-6
No window	1.20	1.39	1.12	1.23	1.24
w/ Lanczos window	1.03	1.04	0.98	0.97	1.07
w/ von Hann window	1.00	0.98	/	/	/
w/ Blackman window	0.92	0.94	0.92	0.92	0.95
w/ Kaiser 50-dB window	0.98	1.02	0.97	0.98	1.05

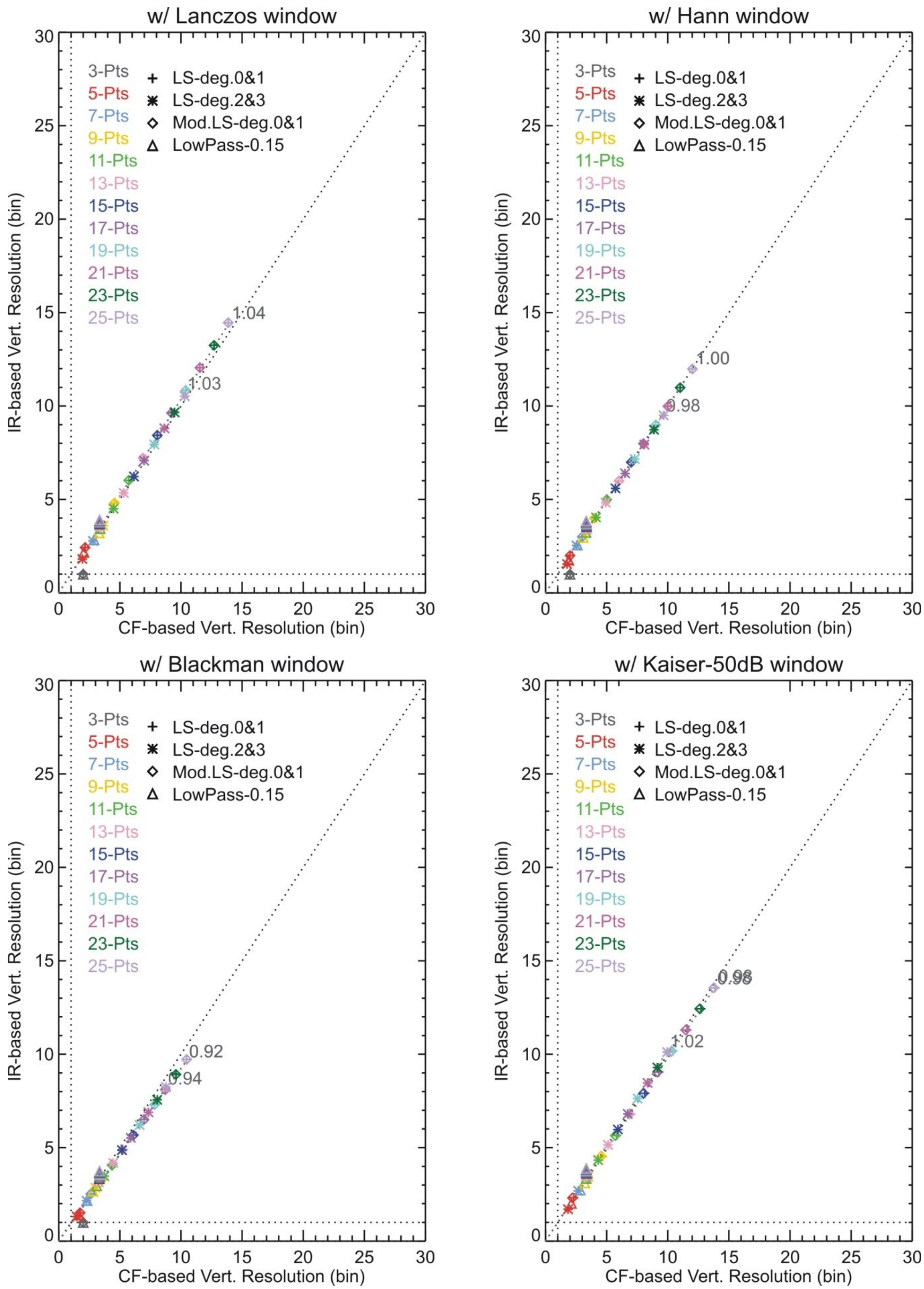

Figure 4.7 Same as Figure 4.5, but the filters being convolved with the four windows introduced in section 2

Figure 4.8 shows, for the filters introduced in **section 2**, the correspondence between the two proposed standardized vertical resolutions (in bins) and the number of filter coefficients used (full-widths comprised between 3 and 25 points). The dashed grey line represents unity slope (i.e., 1 bin for 1 filter coefficient), and the numbers at the end of the red and blue dotted straight lines indicate the slope of the linear fit applied to the paired points for each definition. As expected for a boxcar average, the impulse response-based definition yields a vertical resolution (in bins) that is equal to the number of terms used (see **Figure 2.2**). This is a particular case for which reporting vertical resolution using the number of filter terms yields a result identical to the impulse response-based standardized definition. Note that for low-pass filters with a prescribed cut-off frequency, the vertical resolution does not depend at all on the number of filter terms used (right hand plot).

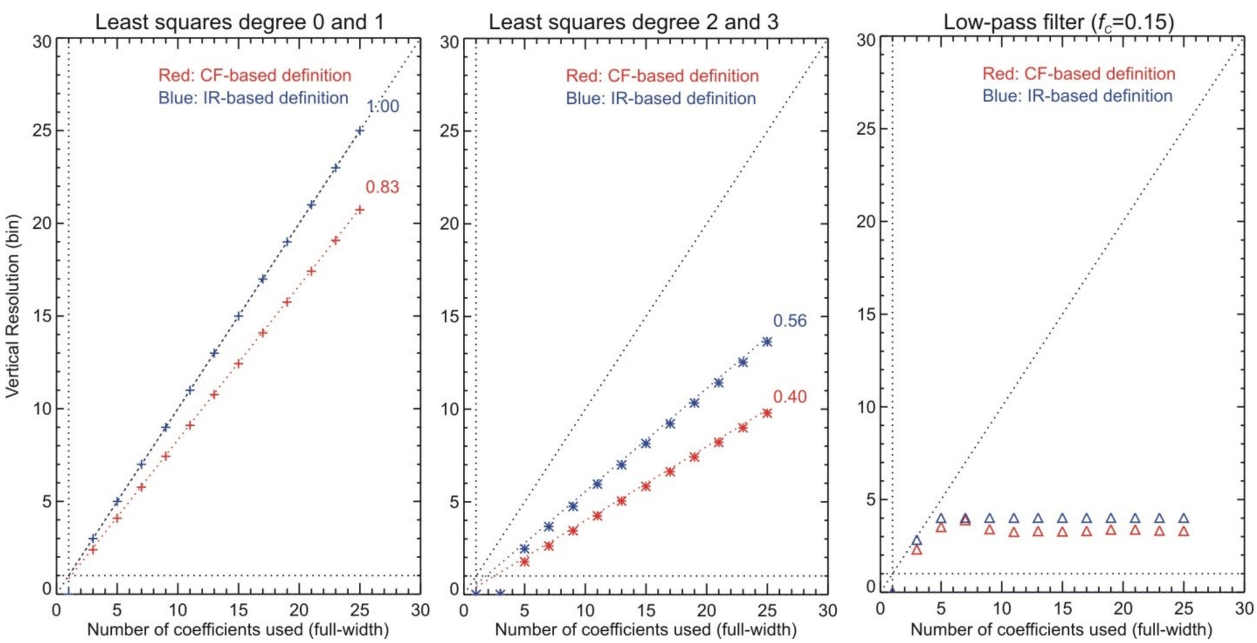

Figure 4.8 Correspondence between cut-off frequency-based (red) and impulse response-based (blue) vertical resolution (in bins), and the number of filter coefficients used (full-width), for 3 filters introduced in section 2. The dashed grey line represents unity slope (i.e., 1 bin for 1 point), and the numbers at the end of the red and blue dotted straight lines indicate the slope of the linear fit applied to the paired points for each definition

Figure 4.9 is similar to **Figure 4.8**, this time after convolution by a von Hann window. Interestingly, this time the cut-off frequency-based definition yields a vertical resolution (in bins) equal to the number of terms used for the boxcar average. This is another particular case, this time a case for which reporting vertical resolution using the number of filter terms yields a result identical to the cut-off frequency-based standardized definition.

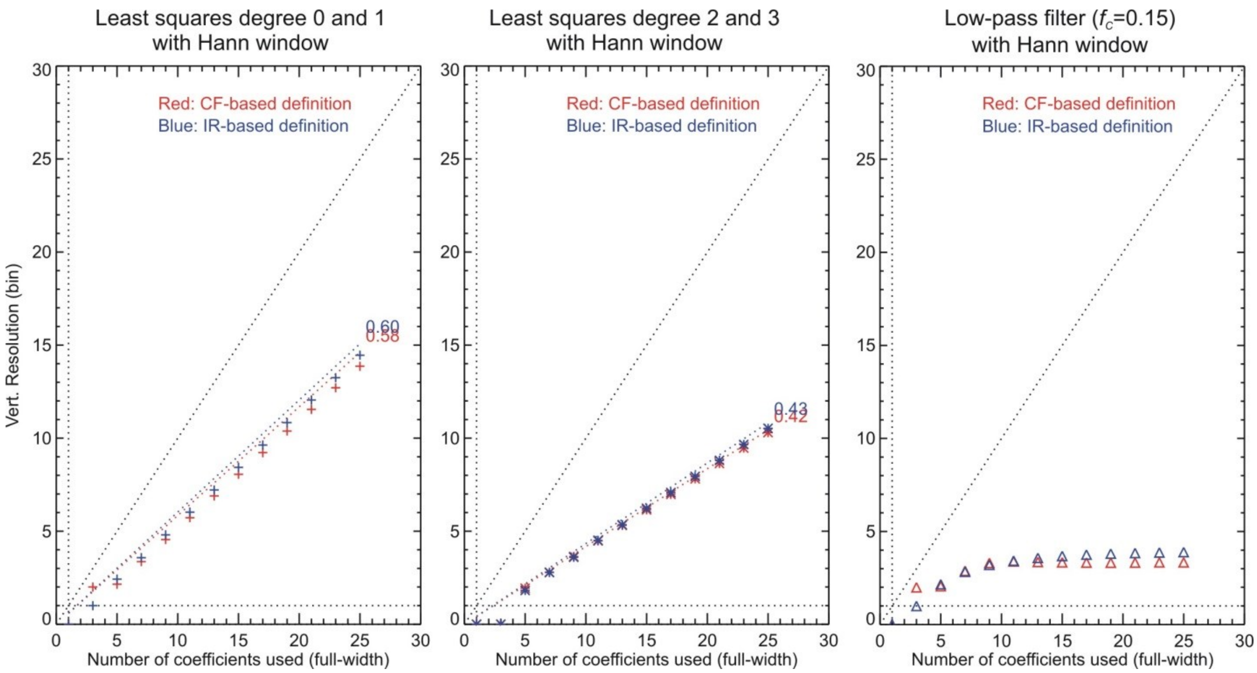

Figure 4.9 Same as Figure 4.8 this time after convolution by a von Hann window

Figure 4.10 is similar to **Figure 4.8**, but for three selected derivative filters. The third filter (right hand side) was chosen because once again the cut-off frequency-based definition yields a vertical resolution (in bins) that is equal to the number of filter terms used (Savitsky-Golay filter derivative, degree 3 or 4).

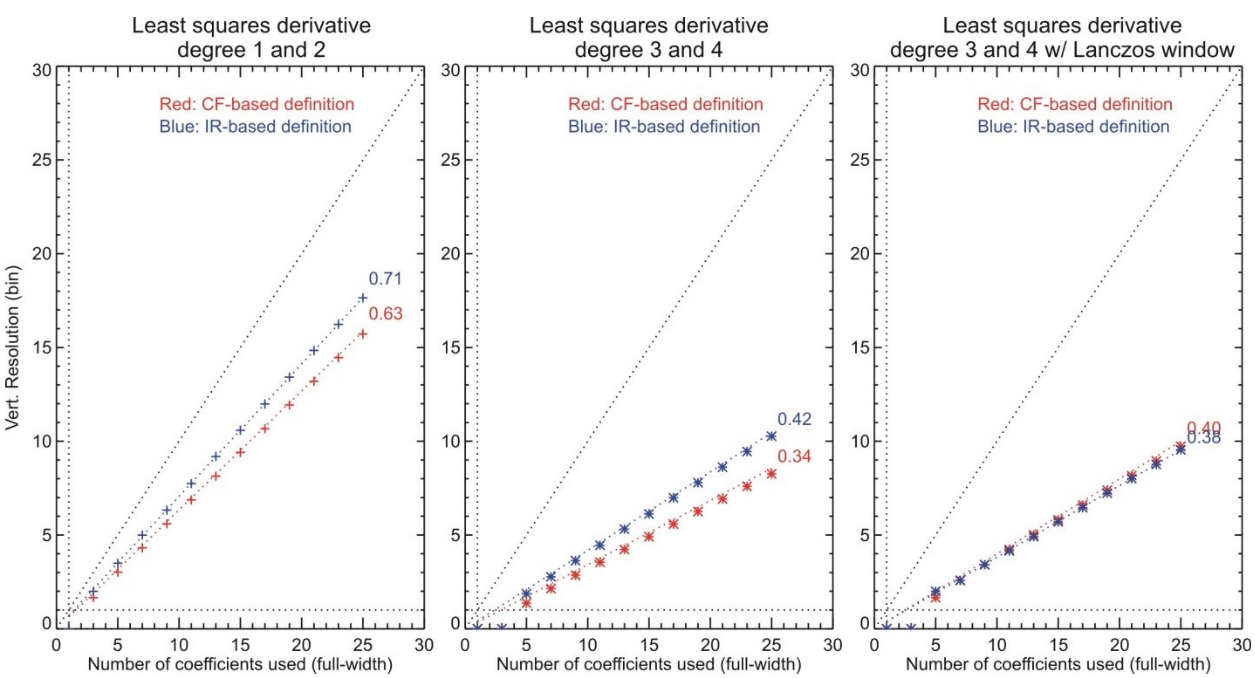

Figure 4.10 Same as Figure 4.8 but for selected derivative filters and windows

The factors between the vertical resolutions (in bins) and the number of filter coefficients are compiled in **Table 4.2** and **Table 4.3** for the cut-off frequency-based and the impulse response-based definition respectively.

Table 4.2 Proportionality factor between the number of filter coefficients (full-width) and vertical resolution based on cut-off frequency (in bins) for the filters and windows introduced in section 2

Ratio $\Delta m_{FC}/(2N+1)$	LS and MLS deg. 0-1	LS deg. 2-3	LS deriv. deg. 1-2	LS deriv. deg. 3-4	LS derive. deg. 5-6
No window	0.83	0.40	0.63	0.34	0.26
w/ Lanczos window	0.58	0.42	0.51	0.40	0.30
w/ von Hann window	0.50	0.43	/	/	/
w/ Blackman window	0.43	0.36	0.40	0.35	0.30
w/ Kaiser 50-dB window	0.57	0.41	0.50	0.39	0.30

Table 4.3 Proportionality factor between the number of filter coefficients (full-width) and vertical resolution based on impulse response FWHM (in bins) for the filters and windows introduced in section 2

Ratio $\Delta m_{IR}/(2N+1)$	LS and MLS deg. 0-1	LS deg. 2-3	LS deriv. deg. 1-2	LS deriv. deg. 3-4	LS derive. deg. 5-6
No window	1.00	0.56	0.71	0.42	0.33
w/ Lanczos window	0.60	0.43	0.50	0.38	0.32
w/ von Hann window	0.50	0.39	/	/	/
w/ Blackman window	0.41	0.34	0.37	0.31	0.29
w/ Kaiser 50-dB window	0.56	0.42	0.49	0.37	0.31

In this section, it was shown that each recommended definition of vertical resolution yields its own numerical values, i.e., for a same set of filter coefficients, the reported standardized vertical resolution will likely have two different numerical values, depending on the definition used. Unfortunately there is no simple proportionality factor between the two definitions that could be used for all digital filters in order to obtain a "unified" homogenous definition yielding identical values. However, after reviewing this homogeneity problem, the ISSI Team concluded that both definitions should still be recommended because the computed values remain close (i.e., within 10% if using windows and within 20% if not using windows), and because each definition is indeed useful for specific applications. For example, the cut-off frequency-based definition is particularly useful for gravity waves studies from lidar temperature measurements, because it can provide, through the transfer function, spectral information that can help interpreting quantitative findings on the amplitude and wavelength of lidar-observed waves. This type of information is not available when using the impulse response-based definition. On the other hand, the impulse response-based definition is widely used in atmospheric remote sensing, and provides information in the physical domain similar to that provided through the averaging kernels of optimal estimation methods used for passive measurements (e.g., microwave measurement of ozone).

The ISSI Team is well-aware that the slight difference in the values computed using the two recommended definitions is somewhat problematic for a smooth NDACC-wide implementation, as well as to ensure proper traceability. For this reason, the ISSI Team strongly recommends that ample meta-information be provided to the data users. In particular, reporting both definitions and explaining the differences between them will help addressing the problem.

4.4 Additional recommendations to ensure full traceability

When archiving the ozone or temperature profiles, reporting values of vertical resolution using a standardized definition such as Δz_{FC} or Δz_{IR} constitutes an important improvement from other, non-standardized, methods such as the number of points used by the filter. However, using one standardized definition or even both standardized definitions proposed here, still does not characterize the complete smoothing effect the filter has on the signal. For full traceability, it is necessary to provide for each altitude point, either the set of filter coefficients used (for one-time smoothing cases) or to provide the complete transfer function or impulse response. This information can be critical when comparing the lidar profiles with profiles from other instruments, or when working with averaging kernels used for other measurements.

If the data provider chooses to report standardized vertical resolution information based on the impulse response definition, the complete vertical resolution information should include:

1) A vector Δz_{IR} of length nk containing the standardized vertical resolution values at each altitude, as proposed in **section 4.2**
2) A two-dimensional array of size nk x nm containing the full impulse response used to estimate the FWHM, as described in **section 2** (nm=2M+1 is the full-length of the impulse function convolved with the filter coefficients, and a recommended value is nm=nk)
3) A vector m of length nm containing the distance (in bins) from the central bin at which the response is reported
4) Meta data information describing clearly the nature of the reported vectors and arrays

If the data provider chooses to report standardized vertical resolution information based on the cut-off frequency definition, the complete vertical resolution information should therefore include:

1) A vector Δz_{FC} of length nk containing the standardized vertical resolution values at each altitude, as proposed in **section 4.1**
2) A two-dimensional array of size nk x nf containing the gain used to estimate the cut-off frequency, as described in **section 2** (nf is the number of frequencies used when applying a Laplace transform to the filter coefficients, and a recommended value is nf=nk)
3) A vector f of length nf containing the values of frequency at which the gain is reported
4) Meta data information describing clearly the nature of the reported vertical resolution vector, frequency vector, and two-dimensional gain array

If the data provider chooses to report standardized vertical resolution based on both the impulse response definition and the cut-off frequency definition, the complete vertical resolution information should include:

1) A vector Δz_{IR} of length nk containing the standardized vertical resolution values at each altitude, as proposed in **section 4.2**

2) A two-dimensional array of size *nk* x *nm* containing the full impulse response used to estimate the FWHM, as described in **section 2** (*nm*=2*M*+1 is the full-length of the impulse function convolved with the filter coefficients, and a recommended value is *nm*=*nk*)
3) A vector *m* of length *nm* containing the distance (in bins) from the central bin at which the response is reported
4) A vector Δz_{FC} of length *nk* containing the standardized vertical resolution values at each altitude, as proposed in **section 4.1**
5) A two-dimensional array of size *nk* x *nf* containing the gain used to estimate the cut-off frequency, as described in **section 2** (*nf* is the number of frequencies used when applying a Laplace transform to the filter coefficients, and a recommended value is *nf*=*nk*)
6) A vector *f* of length *nf* containing the values of frequency at which the gain is reported
7) Meta data information describing clearly the nature of all reported vectors and arrays

4.5 Practical implementation within NDACC

Numerical tools were developed and provided to the NDACC PIs in order to facilitate the implementation of the network-wide use of the proposed standardized definitions. These tools consist of easy-to-use plug-in routines written in IDL, MATLAB and FORTRAN, which convert a set of filter coefficients into the needed standardized values of vertical resolution following one or the other proposed definitions. The tools are written in such a way that they can be called in the NDACC PI's lidar data processing algorithm each time a smoothing and/or differentiating operation occurs. The routines can handle multiple smoothing and/or differentiating operations applied successively throughout the lidar data processing chain, as described in **sections 4.1** and **4.2**.

The routine "NDACC_ResolIR" provides vertical resolution values with a definition based on the FWHM of the filter's impulse response. When the routine is called for the first time in the data processing chain, the sampling resolution and the coefficients of the filter are the only input parameters of the routine. The routine convolves the coefficients with an impulse (delta function for smoothing filters and Heaviside function for derivative filters) to obtain the filter's impulse response, and then identifies the full-width at half-maximum (FWHM) of this response. The response and the value of vertical resolution are the output parameters of the routine. The product of the response full width by the sampling resolution is performed inside the routine. When a second call to the routine occurs (second smoothing occurrence), the vertical resolution output from the first call is no longer used. Instead, the response output from the first call is used as input parameter for the second call, together with the sampling resolution and the coefficients of the second filter. The input response is convoluted with the coefficients of the second filter to obtain a second response. The routine identifies the FWHM of this new response. Once again the vertical resolution is computed inside the routine by calculating the product of the new FWHM and the sampling resolution. The new response and the new vertical resolution are the output parameters of the routine after the second call. The procedure is repeated as many times as needed, i.e., as many times as a smoothing or differentiation operation occurs.

The routine "NDACC_ResolDF" provides vertical resolution values with a definition based on the cut-off frequency of a digital filter. When the routine is called for the first time in the data processing chain, the sampling resolution and the coefficients of the filter are the only input parameters of the routine. The routine applies a Laplace transform to the coefficients to obtain the filter's gain, and then identifies the cut-off frequency. The inverse of twice the cut-off frequency is multiplied by the sampling resolution to obtain the vertical resolution. The gain and the vertical resolution are the output parameters of the routine. When a second call to the routine occurs (i.e., a second smoothing operation occurs), the cut-off width output from the first call is not used anymore. Instead, the gain output from the first call is used as input parameter for the second call, together with the sampling resolution and the coefficients of the second filter. The product of the input gain and gain computed from the second filter is the new gain from which the routine identifies the cut-off frequency. A new vertical resolution is obtained by multiplying the inverse of twice the new cut-off frequency by the sampling resolution. The new gain and the new vertical resolution are the output parameters of the routine after the second call. The procedure is repeated as many times as needed, i.e., as many times as a smoothing or differentiation operation occurs.

The standardization tools became available in summer 2011. They were distributed to several members of the ISSI Team for testing and validation. Their implementation was validated for several NDACC ozone and temperature lidar algorithms. The validation experiments consisted of simulating noisy lidar signals with a forward model, then analyzing the simulated signals using the NDACC data processing algorithms (inverse models). To quantify the effect of the filters used in the algorithms and validate the proper derivation of the standardized vertical resolution therein, the theoretical gain and the actual gain of the filter were compared. The actual gain is the ratio of the Fast Fourier Transform (FFT) of the signals (or profiles) before and after filtering. The theoretical gain is the gain computed by applying the Laplace Transform to the filter coefficients.

An example of such validation experiment is shown for the JPL temperature lidar at Mauna Loa, Hawaii in **Figure 4.11**. The filter in this case is a boxcar average convoluted with a von Hann window (17 points full-width), and the routine to test is NDACC_ResolDF. The experiment consisted of producing 30 sets of noisy simulated lidar signals (blue curve, left plot), then analyzing the signals to retrieve temperature (red curve, left plot). The observed gain (blue curve, right plot) is an average of the 30 gains obtained by calculating the ratio of the FFT of each smoothed profile to the corresponding unsmoothed profile. The theoretical gain (red curve, right plot) was obtained by applying a Laplace Transform to the filter coefficients. The theoretical and observed gain curves agree very well, especially in the transition region and at the location of the cut-off frequency, thus validating the proper implementation of the routine into this particular algorithm. In this particular case, the cut-off frequency f_C has a value of 0.0625, which when inversed, yields 16 bins (i.e., interval including 17 points, consistent with the left plot of **Figure 4.9**). Using a sampling resolution of 300-m (see **Figure 4.11** left plot) the vertical resolution is therefore 4.8 km.

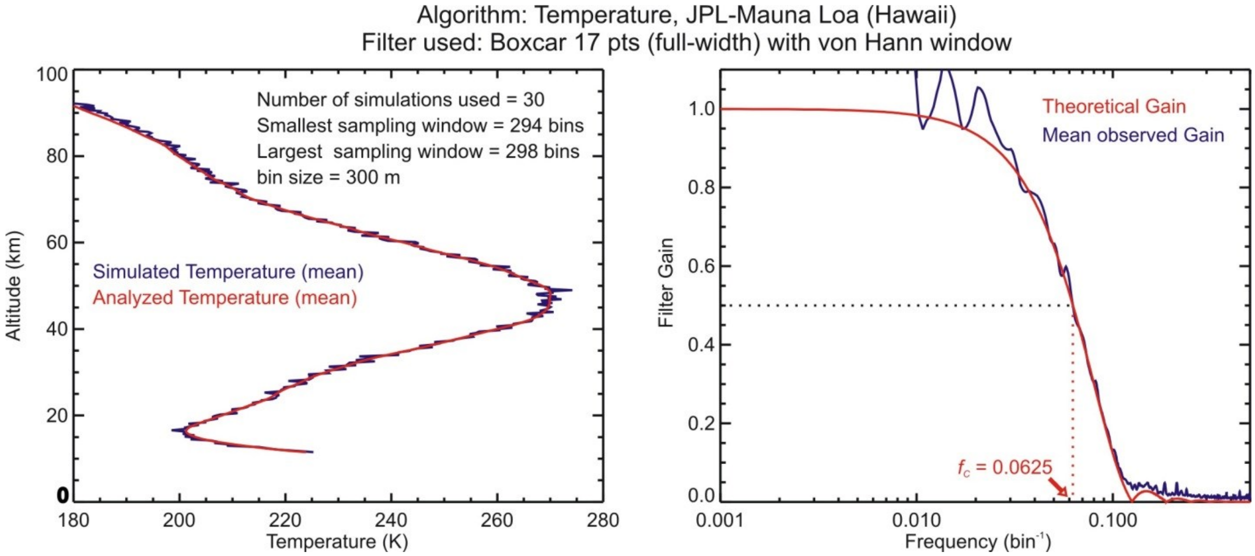

Figure 4.11 Results of the validation of the routine NDACC_ResolDF implemented in the JPL temperature lidar algorithm for the NDACC station of Mauna Loa. Left: unfiltered, noisy simulated profile (blue) and retrieved, filtered profile (red); Right: observed gain (blue) and theoretical gain (red). A boxcar average convolved with a von Hann window (17-points full-width) is used in this case (see text for details)

Another example of validation is shown in **Figure 4.12** (RIVM stratospheric ozone lidar in Lauder, New Zealand). The derivative filter in this case is a least-squares fit using a polynomial of degree 1 (5 points full-width), and the routine being tested is NDACC_ResolIR. The experiment consisted of producing simulated lidar signals for an ozone profile that included a delta peak perturbation of 100% amplitude at 30 km altitude (blue curve, left plot), then analyzing the signals to retrieve ozone (red curve, left plot). The observed response (blue curve, right plot) is obtained by calculating the FWHM of the resulting perturbation in the smoothed profile. The theoretical response (red curve, right plot) was obtained by convolving a Heaviside step function with the filter coefficients. The theoretical and observed response curves agree very well, especially their FWHM, thus validating the proper implementation of the routine into this particular algorithm.

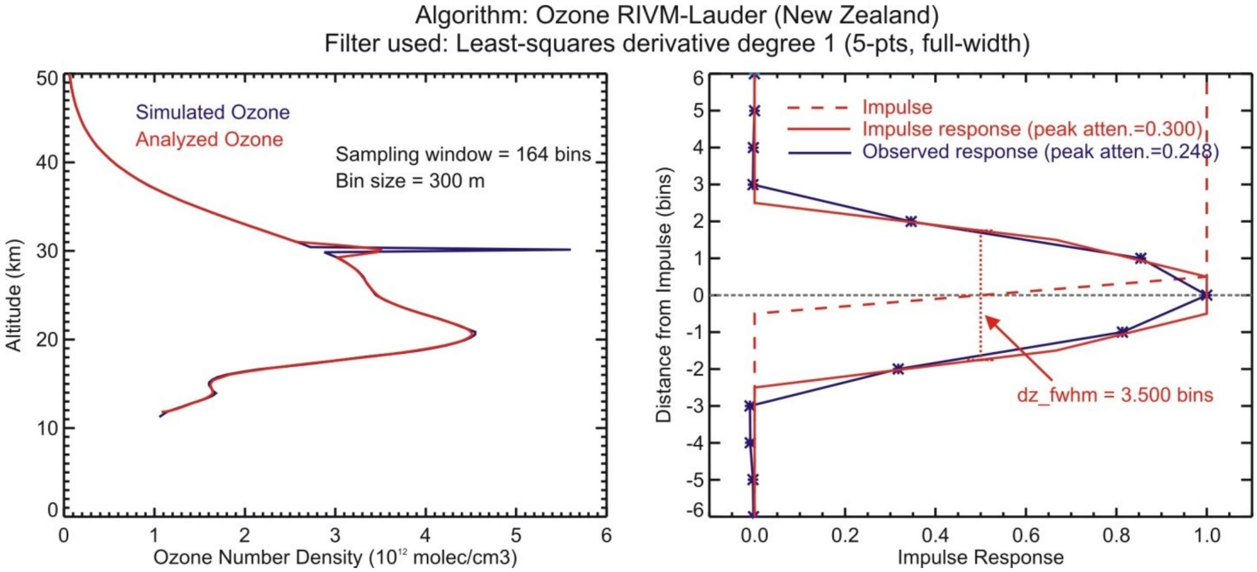

Figure 4.12 Same as Figure 4.11 but for NDACC_ResolIR implemented in the RIVM stratospheric ozone lidar algorithm for the NDACC station of Lauder. Left: unfiltered, simulated profile including an impulse perturbation of 100% at 30 km (blue), and retrieved, filtered profile (red); Right: observed response (blue) and theoretical response (red). A least-squares polynomial of degree 1 (5-points full-width) is used in this case (see text for details)

A third example of validation is shown in **Figure 4.13** for the tropospheric ozone lidar at Reunion Island, France. Once again a good agreement between the observed and theoretical gain curves demonstrate that the routine NDACC_ResolDF was successfully implemented in the Reunion island tropospheric ozone lidar data processing algorithm.

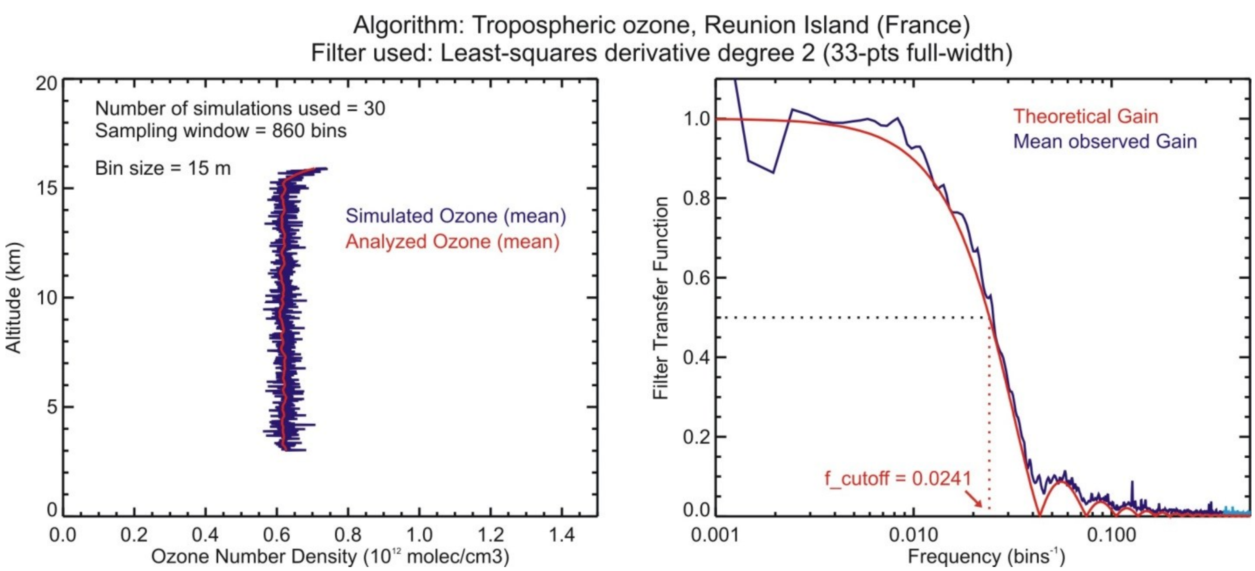

Figure 4.13 Same as Figure 4.11 but for NDACC_ResolDF implemented in the tropospheric ozone lidar algorithm for the NDACC station of Reunion Island (see text for details)

Acknowledgements

This work was initiated in response to the 2010 Call for International Teams of Experts in Earth and Space Science by the International Space Science Institute (ISSI) in Bern, Switzerland. It could not have been performed without the travel and logistical support of ISSI. Part of the work described in this report was carried out at the Jet Propulsion Laboratory, California Institute of Technology, under agreements with the National Aeronautics and Space Administration. Part of this work was carried out in support of the VALID Project. RJS would like to acknowledge the support of the Canadian National Sciences and Engineering Research Council for support of The University of Western Ontario lidar work.

References

Argall, P. S.: Upper altitude limit for Rayleigh lidar, Ann. Geophys., 25, 19-25, 10.5194/angeo-25-19-2007, 2007

Beyerle, G., and McDermid, I. S.: Altitude Range Resolution of Differential Absorption Lidar Ozone Profiles, Appl. Opt., 38, 924-927, 1999.

Birge, R. T., and Weinberg, J. W.: Least-Squares' Fitting of Data by Means of Polynomials, Rev. Mod. Phys., 19, 298, 1947

Eisele, H., and Trickl, T.: Improvements of the aerosol algorithm in ozone lidar data processing by use of evolutionary strategies, Appl. Opt., 44, 2638-2651, 2005

Godin, S., Carswell, A. I., Donovan, D. P., Claude, H., Steinbrecht, W., McDermid, I. S., McGee, T. J., Gross, M. R., Nakane, H., Swart, D. P. J., Bergwerff, H. B., Uchino, O., von der Gathen, P., and Neuber, R.: Ozone Differential Absorption Lidar Algorithm Intercomparison, Appl. Opt., 38, 6225-6236, 1999.

Godin-Beekmann, S., Porteneuve, J., and Garnier, A.: Systematic DIAL lidar monitoring of the stratospheric ozone vertical distribution at Observatoire de Haute-Provence (43.92 degrees N, 5.71 degrees E), J. Environ. Monit., 5, 57-67, 10.1039/b205880d, 2003

Gross, M. R., McGee, T. J., Ferrare, R. A., Singh, U. N., and Kimvilakani, P.: Temperature measurements made with a combined Rayleigh-Mie and Raman lidar, Appl. Opt., 36, 5987-5995, 1997

Hamming, R. W.: Digital Filters, Third Edition ed., Prentice Hall, Englewood Cliffs, New Jersey, 1989

Hinkley, E. D.: Laser monitoring of the atmosphere, Topics in applied physics, 14, Springer-Verlag, 380 pp., 1976

Kaiser, J. F., and Reed, W. A.: Data smoothing using low-pass digital-filters, Rev. Sci. Instr., 48, 1447-1457, 1977

Kempfer, U., Carnuth, W., Lotz, R., and Trickl, T.: A wide-range ultraviolet lidar system for tropospheric ozone measurements: Development and application, Rev. Sci. Instr., 65, 3145-3164, 10.1063/1.1144769, 1994

Knuth, D. E.: Faulhaber,Johann and sums of powers, Math. Comp., 61, 277-294, 10.2307/2152953, 1993

Leblanc, T., McDermid, I. S., and Walsh, T. D.: Ground-based water vapor raman lidar measurements up to the upper troposphere and lower stratosphere for long-term monitoring, Atmos. Meas. Tech., 5, 17-36, 10.5194/amt-5-17-2012, 2012

Savitzky, A., and Golay, M. J. E.: Smoothing and differentiation of data by simplified least squares procedures, Anal. Chem., 36, 1627-&, 1964

Sica, R. J., and Russell, A. T.: Measurements of the effects of gravity waves in the middle atmosphere using parametric models of density fluctuations. Part I: Vertical wavenumber and temporal spectra, J. Atmos. Sci., 56, 1308-1329, 1999

Sica, R. J., and Haefele, A.: Retrieval of temperature from a multiple-channel Rayleigh-scatter lidar using an optimal estimation method, Appl. Opt., 54, 1872-1889, 10.1364/ao.54.001872, 2015

Steinier, J., Termonia, Y., and Deltour, J.: Smoothing and differentiation of data by simplified least square procedure, Anal. Chem., 44, 1906-1909, 10.1021/ac60319a045, 1972

Swart, D. P. J., Apituley, A., Spakman, J., Visser, E. P., and Bergwerff, H. B.: RIVMs tropospheric and stratospheric ozone lidars for European and global monitoring networks, Proceedings of the 17th International Laser Radar Conference, Laser Radar Society of Japan, Sendaı¨, Japan, 1994, 405-408, 1994

Trickl , T.: Tropospheric trace-gas measurements with the differential-absorption lidar technique, pp. 87-147 in: Recent Advances in Atmospheric Lidars, L. Fiorani, V. Mitev, Eds., INOE Publishing House, Bucharest (Romania, 2010), Series on Optoelectronic Materials and Devices, Vol. 7, ISSN 1584-5508, ISSN 978-973-88109-6-9; a revised version is available from the author

VDI Guideline 4210, Verein Deutscher Ingenieure, Düsseldorf, Germany, 1999

Vogelmann, H., and Trickl, T.: Wide-range sounding of free-tropospheric water vapor with a differential-absorption lidar (DIAL) at a high-altitude station, Appl. Opt., 47, 2116-2132, 10.1364/ao.47.002116, 2008

List of abbreviations

DIAL	differential absorption lidar
FWHM	full width at half maximum
FFT	Fourier forward transformation
OHP	Observatoire Haute Provence
ISSI	International Space Science Institute
LS	least squares
NDACC	Network for the detection of atmospheric composition change
NER(D)	near-equal-ripple (derivative)
OEM	optimal estimation method
PI	principal investigator
sqrt	square root
VDI	Association of German engineers (Verein Deutsche Ingenieure)